Distance constraints on activation of TRPV4 channels by AKAP150-bound PKCα in arterial myocytes

Sendoa Tajada,[1] Claudia M. Moreno,[1] Samantha O'Dwyer,[1] Sean Woods,[1] Daisuke Sato,[2] Manuel F. Navedo,[2] and L. Fernando Santana[1]

[1]Department of Physiology and Membrane Biology and [2]Department of Pharmacology, University of California Davis School of Medicine, Davis, CA

TRPV4 (transient receptor potential vanilloid 4) channels are Ca^{2+}-permeable channels that play a key role in regulating vascular tone. In arterial myocytes, opening of TRPV4 channels creates local increases in Ca^{2+} influx, detectable optically as "TRPV4 sparklets." TRPV4 sparklet activity can be enhanced by the action of the vasoconstrictor angiotensin II (AngII). This modulation depends on the activation of subcellular signaling domains that comprise protein kinase C α (PKCα) bound to the anchoring protein AKAP150. Here, we used super-resolution nanoscopy, patch-clamp electrophysiology, Ca^{2+} imaging, and mathematical modeling approaches to test the hypothesis that AKAP150-dependent modulation of TRPV4 channels is critically dependent on the distance between these two proteins in the sarcolemma of arterial myocytes. Our data show that the distance between AKAP150 and TRPV4 channel clusters varies with sex and arterial bed. Consistent with our hypothesis, we further find that basal and AngII-induced TRPV4 channel activity decays exponentially as the distance between TRPV4 and AKAP150 increases. Our data suggest a maximum radius of action of ∼200 nm for local modulation of TRPV4 channels by AKAP150-associated PKCα.

INTRODUCTION

The function of arteries and arterioles is to deliver the blood pumped by the heart to organs. Smooth muscle cells lining the walls of these vessels have an intrinsic ability to contract in response to increases in intravascular pressure (Bayliss, 1902). This behavior, termed the myogenic response, is initiated by stretch-induced activation of nonselective cation channels of the transient receptor potential family, including TRPP2, TRPC6, and TRPM4, which depolarize arterial myocytes (Welsh et al., 2002; Earley et al., 2004; Spassova et al., 2006; Narayanan et al., 2013; Gonzales et al., 2014). Membrane depolarization, in turn, activates voltage-gated L-type $Ca_V1.2$ channels (Harder et al., 1987; Fleischmann et al., 1994; Rubart et al., 1996; Jaggar et al., 1998; Knot and Nelson, 1998). The resulting influx of Ca^{2+} via a single $Ca_V1.2$ channel produces a local elevation in intracellular Ca^{2+} that can be detected optically in the form of a "$Ca_V1.2$ sparklet" (Navedo et al., 2005, 2007; Amberg et al., 2007). Activation of multiple $Ca_V1.2$ sparklets induces a global increase in intracellular Ca^{2+} concentration ($[Ca^{2+}]_i$) that activates myosin light chain kinase, thus initiating contraction. This myogenic response is critical for the process of autoregulation of blood flow by resistance vessels.

As is the case with other important physiological processes, the myogenic response varies between females and males. For example, cerebral, coronary, and cochlear arteries from male rodents have a higher level of myogenic tone than the same arteries from females (Wellman et al., 1996; Geary et al., 2000a,b). Although multiple studies have demonstrated that the endothelium is a major contributor to sex-specific differences in arterial and arteriolar function (Wellman et al., 1996; Lamping and Faraci, 2001; Sader and Celermajer, 2002; Villar et al., 2008; Chrissobolis and Faraci, 2010), whether smooth muscle contributes to these differences is unclear.

Several studies have suggested higher expression of PKC in male than female aortic smooth muscle (Kanashiro and Khalil, 2001; Maddali et al., 2005). One protein that is expressed in vascular smooth muscle cells and is subject to regulation by PKCα is the TRPV4 (transient receptor potential vanilloid 4) channel. Like $Ca_V1.2$ channels, TRPV4 channels are permeable to Ca^{2+} and produce analogous local Ca^{2+}-signaling events termed "TRPV4 sparklets" (Liedtke et al., 2000; Strotmann et al., 2000; Sonkusare et al., 2012; Mercado et al., 2014). TRPV4 sparklets reflect a degree of Ca^{2+} entry that exceeds that of $Ca_V1.2$ sparklets by ∼100-fold (Mercado et al., 2014). However, because basal TRPV4 sparklet activity in arterial myocytes is very low, these events do not increase global $[Ca^{2+}]_i$ and thus do not contribute to contraction.

Correspondence to L. Fernando Santana: lfsantana@ucdavis.edu

Abbreviations used: 11,12-EET, 11,12-epoxyeicosatrienoic acid; BK, Ca^{2+}-activated K^+; DAG, diacylglycerol; FWHM, full width half maximum; GSD, ground state depletion; Mg^{2+}-PSS, Mg^{2+}–physiological salt solution; TIRF, total internal reflection fluorescence.

The Rockefeller University Press $30.00
J. Gen. Physiol. 2017 Vol. 149 No. 6 639–659
https://doi.org/10.1085/jgp.201611709

Instead, TRPV4 channels in these cells have been linked to relaxation through a mechanism in which activation of TRPV4 channels by the endothelium-derived factor 11,12-epoxyeicosatrienoic acid (11,12-EET) results in an influx of Ca^{2+} that activates nearby ryanodine receptors (Earley et al., 2005, 2009). These receptors then release Ca^{2+} from the SR in the form of a local Ca^{2+} spark, which activates juxtaposed large-conductance, Ca^{2+}-activated K^+ (BK) channels in the plasma membrane (Nelson et al., 1995). This results in membrane hyperpolarization and closure of $Ca_V1.2$ channels, thereby decreasing $[Ca^{2+}]_i$ and causing myocyte relaxation.

TRPV4 channels are activated by exposure of smooth muscle cells to the vasoconstrictor angiotensin II (AngII; Mercado et al., 2014), which acts through activation of heteromeric G_q proteins to increase diacylglycerol (DAG) levels, leading to stimulation of PKCα activity. PKCα is targeted to the sarcolemma of vascular smooth muscle cells by the scaffolding protein AKAP150. Indeed, both AKAP150 and PKCα are necessary for acute and chronic AngII-induced changes in Ca^{2+} signaling and myogenic tone (Navedo et al., 2008; Nieves-Cintrón et al., 2008; Nystoriak et al., 2014). Although the concept that TRPV4 channels are locally controlled by AKAP150-associated proteins has been demonstrated in several cell types, including endothelial cells and vascular smooth muscle cells (Fan et al., 2009; Mercado et al., 2014; Sonkusare et al., 2014), a fundamental, yet unanswered, question is how close must these proteins be to one another for effective signaling.

In this study, we sought to provide a quantitative answer to this difficult question by investigating the spatial and functional organization of TRPV4 channels in vascular smooth muscle cells using a combination of total internal reflection fluorescence (TIRF) imaging and super-resolution nanoscopy. Applying a multipronged approach, we determined TRPV4 channel activity in myocytes from mesenteric arteries, pial arteries, and parenchymal arterioles (hereafter referred to as mesenteric, pial, and parenchymal myocytes, for simplicity) isolated from female and male mice. We also determined the distance between AKAP150 and TRPV4 clusters in these cells using super-resolution microscopy. Our data suggest that basal and AngII-induced TRPV4 sparklet activity varies depending on the vessel from which the cells were obtained as well as the sex of the animal. Indeed, overall TRPV4 sparklet activity was lower in pial and parenchymal myocytes from female than male mice and surprisingly was undetectable in mesenteric myocytes from animals of either sex. An analysis of super-resolution images and TRPV4 sparklet data suggests that TRPV4 channel activity decays exponentially as the distance between TRPV4 and AKAP150 increases. Indeed, our data indicate a critical cutoff of ~200 nm for local modulation of TRPV4 channels by AKAP150-associated PKCα.

MATERIALS AND METHODS

Isolation of myocytes from pial and mesenteric arteries and parenchymal arterioles

Male and female WT C57BL/6J (The Jackson Laboratory) and AKAP150 null ($AKAP150^{-/-}$) mice were used in this study. Animals were euthanized by decapitation after intraperitoneal administration of a lethal dose of sodium pentobarbital (250 mg/kg). All experiments were conducted in accordance with the University of California Institutional Animal Care and Use Committee guidelines. Myocytes for TIRF and super-resolution microscopy were dissociated from pial cerebral arteries, parenchymal cerebral arterioles, and mesenteric arteries using previously described approaches (Navedo et al., 2005; Tajada et al., 2013; Li et al., 2014; Mercado et al., 2014).

In brief, for pial (basilar, posterior, and mid-cerebral) arteries, the brain was rapidly removed from the skull and placed in cold Mg^{2+}–physiological salt solution (Mg^{2+}-PSS; 140 mM NaCl, 5 mM KCl, 2 mM $MgCl_2$, 10 mM HEPES, and 10 mM glucose), adjusted to pH 7.4 with NaOH. Pial arteries were dissected out, cleaned of connective tissue, and incubated for 8 min at 37°C in Mg^{+2}-PSS supplemented with 0.3 mg/ml papain (Worthington Biochemical Corporation) and 0.3 mg/ml dithiothreitol (DTT; Sigma-Aldrich), followed by a second incubation (5 min at 37°C) in Mg^{2+}-PSS supplemented with 0.3 mg/ml type F and 0.7 mg/ml type H collagenase (Sigma-Aldrich). Arteries were then washed with Mg^{2+}-PSS and kept on ice in the same solution for 30 min, after which cells were gently triturated with a fire-polished Pasteur pipette to yield a single-cell suspension.

Parenchymal arterioles were cut near their junction to the mid-cerebral artery. The arachnoid mater around the middle cerebral artery was gently removed from the brain such that parenchymal arterioles remained attached to the middle cerebral artery. Arterioles were dissected in cold MOPS-buffered saline solution (145 mM NaCl, 5 mM KCl, 1 mM $MgSO_4$, 2.5 mM $CaCl_2$, 1 mM KH_2PO_4, 3 mM MOPS, 2 mM pyruvate, 5 mM glucose, and 1% BSA, pH 7.4). Arteriole segments were then placed in a glutamate isolation solution (55 mM NaCl, 5.6 mM KCl, 80 mM Na-glutamate, 2 mM $MgCl_2$, 10 mM HEPES, and 10 mM glucose), adjusted to pH 7.3 with NaOH, and incubated first in 0.5 mg/ml papain and 1.0 mg/ml dithioerythritol (DTE; Sigma-Aldrich) for 11 min at 37°C, and then in 1.0 mg/ml collagenase type F for 13 min at 37°C. The digested segments were washed three times in ice-cold glutamate isolation solution and incubated on ice in the same solution for 30 min. Digested arterioles were gently triturated to dissociate smooth muscle cells and stored in ice-cold glutamate isolation solution until used.

Third-order mesenteric arteries were dissected out, placed in an ice-cold smooth muscle dissociation solution (145 mM NaCl, 4.2 mM KCl, 0.6 mM KH_2PO_4, 1.2 mM $MgCl_2$, 10 mM HEPES, and 11 mM glucose), adjusted to pH 7.4 with NaOH, and carefully cleaned of adipose and connective. Arteries were cut into small segments and then placed in dissociation solution supplemented with 0.5 mg/ml papain, 1 mg/ml BSA (Sigma-Aldrich), and 1 mg/ml DTE, and incubated for 9–15 min at 37°C. This was followed by a second 12- to 16-min incubation in dissociation solution containing 10 µM Ca^{2+}, 0.6 mg/ml collagenase F, and 1 mg/ml BSA. After rinsing the arteries twice with dissociation solution containing 10 µM Ca^{2+}, single cells were obtained by gentle trituration with a wide-bore glass pipette. Cells were maintained at 4°C until used.

Electrophysiology and $[Ca^{2+}]_i$ imaging

After isolation, cells were kept in ice-cold Mg^{2+}-PSS solution for about an hour before TRPV4 currents were recorded. Electrophysiological measurements were recorded at room temperature using the conventional or amphotericin B–perforated patch whole-cell configuration of the patch-clamp technique as described before (Amberg et al., 2003; Mercado et al., 2014). Freshly isolated myocytes were placed directly in the recording chamber and allowed to settle for a few minutes before starting perfusion with the external solution (composed of 134 mM NaCl, 6 mM KCl, 1 mM $MgCl_2$, 2 mM $CaCl_2$, 10 mM glucose, and 10 mM HEPES). Patch pipettes were made from borosilicate glass (2.0 mm O.D.; World Precision) using a P-97 automatic puller (Sutter Instrument); resistances ranged from 4 to 8 MΩ when filled with the internal solution (composed of 110 mM K-aspartate, 30 mM KCl, 10 mM NaCl, 1 mM $MgCl_2$, and 10 mM HEPES). For experiments involving the recording of $[Ca^{2+}]_i$ and I_{TRPV4} in mesenteric myocytes (see Fig. 8), active PKCα (0.1 U/ml; Millipore) was added to the internal solution. The kinase was activated by the inclusion of the DAG analogue 1-oleoyl-2-acetyl-*sn*-glycerol (OAG; 10 µM) and 90 nM free Ca^{2+} in the pipette solution. TRPV4 currents were recorded using an Axopatch 200B patch-clamp amplifier, filtered at 2 kHz (−3 dB, four-pole Bessel filter) and sampled at 10 kHz. Current recordings were digitized with a Digidata 1440A interface using CLAMPEX 10 software (Molecular Devices).

TRPV4 sparklets were recorded in voltage-clamped (membrane potential = −70 mV) arterial myocytes using a through-lens TIRF system built around an inverted Olympus IX-70 microscope equipped with an Olympus PlanApo (60×; NA = 1.49) oil-immersion lens and an Andor iXON EMCCD camera (pixel size = 13 µm). Cells were continuously superfused with a solution with the following composition: 142 mM NaCl, 6 mM KCl, 1 mM $MgCl_2$, 2 mM $CaCl_2$, 10 mM glucose, and 10 mM HEPES, adjusted to pH 7.4. Nifedipine (10 µM; EMD Millipore) was added to eliminate Ca^{2+} influx through L-type calcium channels and thapsigargin (1 µM) to eliminate Ca^{2+} release from the SR. To monitor $[Ca^{2+}]_i$, cells were patch-clamped in the whole-cell configuration using pipettes filled with a solution composed of 100 mM Na-glutamate, 20 mM NaCl, 42 mM mannitol, 1 mM $MgCl_2$, 4 mM Na_2-ATP, 10 mM EGTA, 10 mM HEPES, and 0.2 mM Rhod-2 (Invitrogen), adjusted to pH 7.2 with NaOH. Rhod-2 was excited with a 563-nm laser. Excitation and emission light were separated using the appropriate set of filters.

TIRF images were acquired at a frequency of 100–300 Hz using TILL Image software. Sparklets were detected and analyzed using custom software written in MATLAB (Navedo et al., 2010; Mercado et al., 2014). Fluorescence intensity values were converted to nanomolar units as described previously (Navedo et al., 2005, 2006). Histograms from all $[Ca^{2+}]_i$ records obtained from arterial myocytes were fit to the following multicomponent Gaussian function:

$$N = \sum_{j=1}^{n} a_j * \exp\left[-\frac{(\Delta[Ca^{2+}]i - jq)^2}{2jb}\right],$$

where a and b are constants, and $\Delta[Ca^{2+}]_i$ and q are the change in intracellular Ca^{2+} concentration and the quantal unit of Ca^{2+} influx, respectively. The activity of sparklets was determined by calculating the nP_s of each sparklet site, where n is the quantal level number, and P_s is the probability that a sparklet site is active.

TRPV4 currents were measured before (control) and after the acute application of the hormone AngII (100 nM), TRPV4 channel agonist (GSK1016790A; 100 nM), and antagonist (HC067047; 1 µM). TRPV4 currents and sparklets were recorded from freshly dissociated cells. Control records were obtained at least 5 min after successful conversion to the whole-cell configuration of the patch-clamp technique. This ensured full equilibration between the contents in the pipette solution and the cytosol. Sparklet and current experiments were terminated when the effects of a drug reached steady state. Although in multiple experiments currents and sparklets were recorded over a period of 10–15 min, in some experiments total recording time was extended up to 30 min to verify the stability of the cellular response.

Our perfusion chambers have a low volume (200 µl), ensuring fast solution exchange (<30 s) at our flow rates. Cells were not incubated with any drugs, or hormone, before being placed in our electrophysiology/imaging recording chamber.

Super-resolution microscopy

Myocytes were plated on collagen-coated coverslips (Neuvitro) for 1 h at 4°C and fixed with 4% paraformaldehyde and 0.1% glutaraldehyde in PBS, for 10 min at

room temperature. After washing with PBS, cells were incubated with 0.1% $NaBH_4$ for 5 min at room temperature (aldehyde reduction) and blocked with 20% SEA BLOCK (Thermo Fisher Scientific) and 0.25% Triton X-100 in PBS for 1 h at room temperature. Permeabilized cells were incubated first with rabbit anti-TRPV4 (10 µg/ml; SC-98592; Santa Cruz Biotechnology, Inc.) and goat anti-AKAP150 (10 µg/ml; SC-6446; Santa Cruz Biotechnology, Inc.) primary antibodies (overnight at 4°C), and then with Alexa Fluor 647–conjugated donkey anti-goat (1 µg/ml; Molecular Probes) and Alexa 532–conjugated donkey anti-rabbit (1 µg/ml; Molecular Probes) secondary antibodies (1 h at room temperature). Coverslips were mounted on microscope slides with a round cavity (NeoLab) using MEA-GLOX imaging buffer and then sealed with Twinsil (Picodent). The imaging buffer contained 10 mM MEA, 0.56 mg/ml glucose oxidase, 34 µg/ml catalase, and 10% wt/vol glucose in TN buffer (50 mM Tris-HCl, pH 8, and 10 mM NaCl). tsA-201 cells were processed following the same protocol.

Super-resolution images of TRPV4 and AKAP150 in arterial myocytes and tsA-201 cells were acquired with a Leica Microsystems ground state depletion (GSD) system coupled to a Leica Microsystems DMI6000B inverted microscope. Images were obtained using a 160× HCX PL APO (NA = 1.47) oil-immersion lens and an Andor iXon3 897 EMCCD camera. The Leica Microsystems GSD system is equipped with high-power lasers with measured intensities at the focal plane of 1.4 kW/cm^2 for 488 nm, 2.1 kW/cm^2 for 532 nm, and 2.1 kW/cm^2 for 642 nm. For image analyses, we set an event threshold of 50 events/pixel to eliminate background, nonspecific signals. High-resolution localization images were reconstructed using the coordinates of centroids of these fluorescent particles obtained from >25,000 images.

Super-resolution localization maps of TRPV4 and AKAP150 were determined using the coordinates of centroids obtained by fitting single-molecule fluorescence signals with a two-dimensional Gaussian function using LASAF software (Leica Microsystems). The localization accuracy (i.e., full width half maximum [FWHM]) of the system is limited by the statistical noise of photon counting. Thus, assuming the point-spread functions are Gaussian, the precision of localization is proportional to DLR/$\sqrt{N}$, where DLR is the diffraction-limited resolution of a fluorophore, and N is the mean number of detected photons per switching event (Dempsey et al., 2011). Accordingly, we estimated a theoretical lateral localization accuracy of ∼13 nm for Alexa 647 and ∼16 nm for Alexa 532. Spatial resolution of the GSD microscope was measured using the DNA-PAINT nanoruler method (GATTAquant; Schmied et al., 2014). In brief, we used a 40R nanoruler consisting of immobilized single-stranded DNA strands with three binding sites for complementary ATTO655-labeled single-stranded DNA separated by 40 nm. Drifting was corrected using fiducial markers included in the probe and the GATTAnalysis software. A histogram of the distance between dye molecules was generated using the same software. Using this approach, we experimentally determined the mean distance separating a 40-nm nanoruler to be 42.9 nm with an FWHM amplitude of 23.8 ± 6.8 nm (Fig. S1). This FWHM value is comparable to our calculated lateral localization accuracy.

We performed two important control experiments to test the specificity of our TRPV4 and AKAP150 antibodies (Fig. S2). Super-resolution images were obtained from tsA-201cells expressing TRPV4 and that were exposed to both primary and secondary antibodies or secondary antibody only (Fig. S2, A and B). We also imaged tsA-201cells not transfected with TRPV4 (Fig. S2 C), but exposed to primary and secondary antibodies. We found that the number of photons captured by our camera from cells transfected with TRPV4 was significantly higher (∼20-fold) than from cells not expressing TRPV4, regardless of whether they were exposed to primary and/or secondary antibodies (Fig. S2 D). We also tested our AKAP150 antibody in WT and AKAP150$^{-/-}$ myocytes (Fig. S2, E–G). As with the TRPV4 antibody, the number of photons was significantly higher (∼14.5-fold) in WT myocytes exposed to primary and secondary antibodies than WT cells exposed only to secondary antibody or AKAP150$^{-/-}$ cells exposed to primary and secondary antibodies.

A nearest neighbor analysis was performed to measure the distance between AKAP150 and TRPV4 channels in the super-resolution localization images. We used a region-based identification analysis using CellProfiler software (Jones et al., 2008) and a custom visual basic array. This analysis uses a modular three-step strategy to identify objects on the basis of a previously published algorithm (Wählby et al., 2004). After the object identification step, the distance from the edge of adjacent AKAP150 and TRPV4 clusters was determined.

Western blot analysis

Intact mesenteric and pial arteries were collected as described in the Isolation of myocytes from pial and mesenteric arteries and parenchymal arterioles section above and pooled from multiple mice: two for mesenteric and four for pial. Parenchymal arterioles were not included in these experiments because of limited tissue availability, which made Western blot analysis of protein in these vessels unreliable. Arteries in Mg^{2+}-PSS solution were centrifuged at 10,000 *g* for 10 min at 4°C and resuspended in 40 µl ice-cold RIPA buffer plus protease inhibitors (Complete Mini Protease Inhibitor Cocktail; Thermo Fisher Scientific). Tissue was homogenized by hand on ice in a Dounce homogenizer and mixed with lithium dodecyl sulfate loading buffer with 5% β-mer-

captoethanol. Samples were incubated at 50°C for 30 min, and the total contents were loaded onto a 4%–12% Bis-Tris polyacrylamide gel. Proteins were separated by electrophoresis at 110 V (1.5 h, room temperature) and then wet-transferred to a nitrocellulose membrane at 40 V (overnight, 4°C). Membranes were then washed in Tris-buffered saline (TBS) with 0.05% Tween 20 (TBS-T) and blocked in 3% BSA TBS (overnight, 4°C). Membranes were subsequently incubated with primary antibody: TRPV4 (1:1,000), AKAP150 (1:1,000), or β-actin (1:2,000; 47778 mouse monoclonal; Santa Cruz Biotechnology, Inc.) either overnight at 4°C (TRPV4 and AKAP150) or for 1 h at room temperature (β-actin). Membranes were then rinsed and incubated with the appropriate HRP-conjugated secondary antibody for 1 h at room temperature. After a final wash, the blots were incubated in 2 ml ECL Western Blotting Detection Reagents (RPN2106; GE Healthcare) for 2 min and subsequently exposed to autoradiography film (HyBlot CL; Denville). Densitometry for immunoreactive bands was performed with ImageJ software (National Institutes of Health), and expression was normalized to the β-actin signal for each lane.

To provide further evidence for the specificity of our AKAP150 antibody, we performed Western blots using WT and AKAP150$^{-/-}$ pial arteries. Densitometry analysis of these Western blots showed robust expression of AKAP150 in WT pial arteries and undetectably low levels in AKAP150$^{-/-}$ arteries (Fig. S2). We did see a nonspecific band with an apparent molecular weight of ∼40 kD in the WT and AKAP150$^{-/-}$ Western blots. However, because AKAP150-associated fluorescence signals are at least an order of magnitude higher than background, the impact of this nonspecific signal on our super-resolution analyses is minimal. Full scale Western blots for TRPV4 and AKAP150 were also performed using WT male and female pial and mesenteric preparations. These Western blots show that our approaches can detect differential levels of TRPV4 and AKAP150 expression in these vessels (Fig. S4).

RNAi

The expression of the human homologous for AKAP150, AKAP79, was down-regulated in tsA-201 cells using Stealth RNAi siRNA against AKAP79 (HSS114139; Invitrogen). A low GC content RNAi scramble duplex with no homology to vertebrate transcripts was used as a negative control (12935200; Invitrogen). siRNA and RNAi negative control were dissolved at a concentration of 20 µM in diethylpyrocarbonate-treated water or the dilution/annealing buffer provided by the manufacturer, respectively. siRNA transfection was performed using Lipofectamine 2000 and Opti-MEM reduced serum medium according to the manufacturer's instructions (Invitrogen). In brief, the day before transfection, cells were plated in six-well plates in medium without antibiotics and used at 90% of confluence to minimize toxicity. For each well, 500 pmol siRNA (25 µl from the 20 µM stock) was diluted in 250 µl Opti-MEM (Invitrogen). In a second tube, 5 µl Lipofectamine 2000 (Invitrogen) was mixed with 250 µl Opti-MEM and incubated for 15 min. The dilutions were combined and incubated for another 15 min. Cells were incubated at 37°C in a humidified CO_2 incubator for 48 h. The efficiency of the siRNA was determined by real-time PCR.

RNA extraction and real-time PCR

Total RNA from tsA-201 cells or mouse arteries was isolated and purified by applying 1 ml of TRIzol reagent per sample according to the manufacturer's instructions (Invitrogen). RNA was purified using the RNeasy Mini kit (QIAGEN). Genomic DNA was digested using RNAase-free DNAase (1023460; QIAGEN). For cDNA synthesis, 1 µg total RNA was reverse-transcribed using the qScriptcDNA supermix (84034; Quanta Biosciences, Inc.). For real-time PCR, a cDNA amount equivalent to 15 ng initial RNA was loaded per well and amplified using PowerUP SYBR Green Mastermix (A25742; Applied Biosystems) under the following conditions: 2 min at 50°C initial UDG activation, denaturation for 2 min at 95°C, followed by 40 cycles consisting of 15 s at 95° and 60 s at 60°C. Table S1 summarizes the sets of primers designed for each gene. Fold change in the expression of mRNA for TRPV4 and AKAP150 was calculated using the $2^{-\Delta\Delta CT}$ method taking the geometric mean of the human control genes 18S, GAPDH, and α-actinin as reference in tsA-201 cells and the geometric mean of the mouse genes 18S, hypoxanthine-guanine phosphoribosyl transferase (HPRT), and β-actin in the artery samples.

In silico modeling

We developed a multidimensional mathematical model of TRPV4, AKAP150, and PKCα distribution and activities using experimentally acquired data. The volume simulated for the statistics is 5 µm × 5 µm × 5 µm. The animations (Videos 1, 2, 3, 4, 5, and 6) show a 2-µm × 2-µm × 0.3-µm space. TRPV4 channels and AKAP150 clusters are distributed randomly on the two-dimensional membrane (x-y plane) located at z = 0 µm. The numbers of TRPV4 channels and AKAP150 clusters (i.e., density) were chosen based on experimental values (Table 1). The diffusion of PKCα was simulated with the random walk process. Every time step, PKCα moves $\sqrt{(2*dt*D_{\mathrm{PKC}})}$, where dt is the time step. Therefore, a set of equations to simulate the random walk is

$$\begin{cases} x_{t+1} = x_t + \sqrt{2\ dt\ D_{PKC}}\sin(\theta)\cos(\phi) \\ y_{t+1} = y_t + \sqrt{2\ dt\ D_{PKC}}\sin(\theta)\sin(\phi), \\ z_{t+1} = z_t + \sqrt{2\ dt\ D_{PKC}}\cos(\theta) \end{cases}$$

Table 1. **Summary of super-resolution data**

Parameter	Pial				Parenchymal				Mesenteric			
	Male		Female		Male		Female		Male		Female	
	TRPV4	AKAP150	TRPV4	AKAP150	TRPV4	AKAP150	TRPV4	AKAP150	TRPV4	AKAP150	TRPV4	AKAP150
Cluster density (clusters/μm^2)	9.8 ± 0.3	35.3 ± 0.7	4.3 ± 0.2	26.3 ± 1.0	9.4 ± 0.6	18.3 ± 0.6	11.7 ± 0.6	10.3 ± 0.4	4.4 ± 0.2	8.8 ± 0.2	6.4 ± 0.3	5.2 ± 0.2
Cluster area (nm^2)	1,834 ± 117	1,860 ± 46	1,285 ± 69	2,802 ± 128	1,245 ± 44	2,014 ± 77	1,054 ± 48	1,219 ± 44	1,507 ± 37	1,180 ± 29	1,195 ± 42	1,295 ± 62
TRPV4–AKAP150 overlap (%)	11.5 ± 0.7	11.5 ± 0.7	6.4 ± 1.6	6.4 ± 1.6	4.6 ± 0.7	4.6 ± 0.7	1.2 ± 0.3	1.2 ± 0.3	1.1 ± 0.2	1.1 ± 0.2	0.4 ± 0.02	0.4 ± 0.02
TRPV4–AKAP150 distance (nm)	69 ± 4	69 ± 4	130 ± 3	130 ± 3	120 ± 7	120 ± 7	251 ± 6	251 ± 6	224 ± 7	224 ± 7	347 ± 9	347 ± 9

where θ and ϕ are random numbers between 0 and π, and 0 and 2π, respectively.

We chose dt = 0.01 ms, and the total simulation time is 1,000 ms. The number of active PKCα is equal to the number of AKAP150 clusters. The lifetime of PKCα (τ_{PKC}) was varied from 5–20 ms. We assume that if the distance between PKCα and TRPV4 is less than 10 nm, a sparklet occurs for 10 ms. The TRPV4 channel activity is computed by the product of the number of sparklet and sparklet duration (number of TRPV4 sparklets × TRPV4 sparklet duration). The program codes are written in C++ and simulated in a high-performance computing cluster (24 nodes, Intel Xeon E3-1270, 3.4 GHz, 32 GB random-access memory). Results were visualized using MATLAB.

Chronic AngII infusion

Mice (8–16 wk old) anesthetized with isoflurane (1–5%) were implanted with a micro-osmotic pumps (1002 model; Alzet). The pumps delivered AngII at 1.1 mg/kg/d (Sigma-Aldrich) for 7 d.

Statistics

Data with a normal distribution are presented as mean ± SEM. Two-sample comparisons of parametric data were performed using Student's t test. Multigroup comparisons were performed using ANOVA. A p-value < 0.05 was considered significant.

Online supplemental material

Fig. S1 shows super-resolution images and analysis of the 40-nm nanoruler. Fig. S2 shows negative control experiments showing the specificity of the AKAP150 and TRPV4 antibodies. Fig. S3 shows that TRPV4 cluster size was similar between nonpermeabilized cells exposed to a TRPV4 antibody that binds to the extracellular side of the channel and permeabilized cells incubated with an antibody against the cytosolic side of the channel. Fig. S4 shows that AKAP150 and TRPV4 expression is differentially expressed in parenchymal, pial, and mesenteric arteries. Fig. S5 shows histograms of the measured distances between AKAP150 and TRPV4. Table S1 shows the primers used for real-time PCR. Videos 1, 2, 3, 4, 5, and 6 show three-dimensional simulations of randomly walking PKC and TRPV4 channel activity in male and female pial, parenchymal, and mesenteric myocytes.

RESULTS

TRPV4 currents are larger in male than in female arterial and arteriolar myocytes

We recorded whole-cell TRPV4 current (I_{TRPV4}), defined as the current blocked by the specific TRPV4 antagonist HC067047 (1 µM; Everaerts et al., 2010), in pial, parenchymal, and mesenteric myocytes isolated from male and female mice (Fig. 1). To minimize alterations in $[Ca^{2+}]_i$ and potential dialysis of key intracellular components, we measured currents using the amphotericin B–perforated patch-clamp technique. I_{TRPV4} was recorded during a 1-s voltage ramp from −80 to +80 mV before and after the application of 100 nM AngII, a potent vasoconstrictor that also stimulates TRPV4 channel activity in vascular smooth muscle (Mercado et al., 2014).

We found that I_{TRPV4} was larger in male than in female pial myocytes (Fig. 1, A and D). A similar finding was obtained in comparisons of I_{TRPV4} in male and female parenchymal myocytes (Fig. 1, B and D). Notably, I_{TRPV4} was, on average, indistinguishable from noise in both male and female mesenteric myocytes (Fig. 1, C and D). Our data suggest that application of AngII increased I_{TRPV4} in pial and parenchymal myocytes but not in male or female mesenteric myocytes. Indeed, for both sexes, I_{TRPV4} was larger in pial than parenchymal and mesenteric myocytes whether AngII was present or not (i.e., control). These data suggest that TRPV4 currents in arterial myocytes vary according to the sex of the animal and the specific vascular bed.

TRPV4 sparklet activity is higher in male than female arterial and arteriolar myocytes

We investigated whether differences in TRPV4 channel activity and/or amplitude account for the disparities in

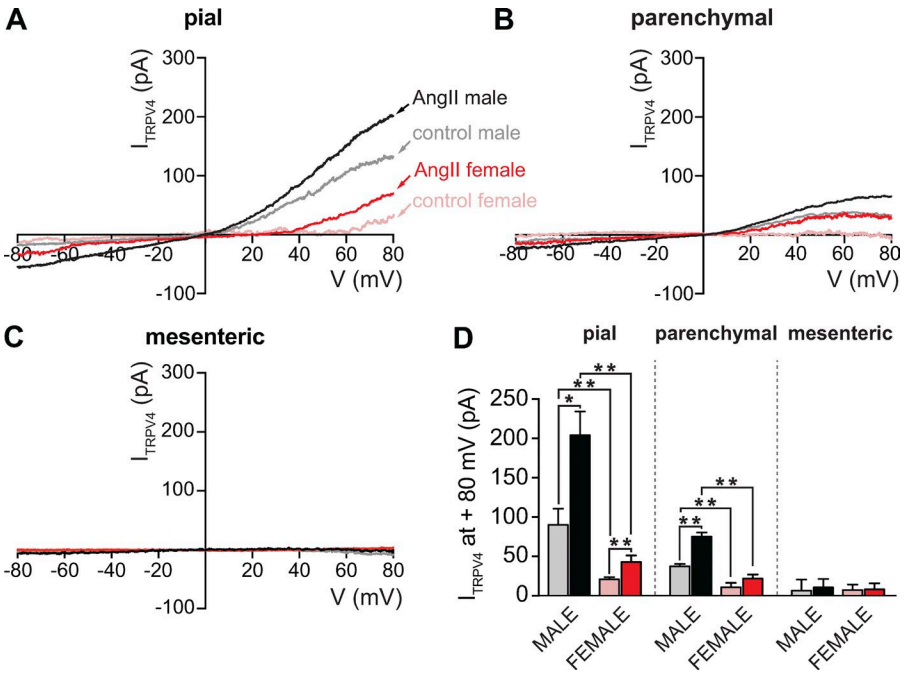

Figure 1. **I_{TRPV4} is larger in male than in female arterial and arteriolar myocytes.** (A–C) Representative I_{TRPV4} obtained in myocytes from pial arteries (A), parenchymal arterioles (B), and mesenteric arteries (C) using the perforated patch/whole-cell configuration of the patch-clamp technique. I_{TRPV4} was defined as the HC067047-sensitive current (1 µM; control). I_{TRPV4} was obtained by subtracting current traces evoked by voltage ramps in the presence of HC067047 from traces in control conditions or in the presence of 100 nM AngII. (D) Bar plot showing mean ± SEM I_{TRPV4} amplitudes at 80 mV in the presence and absence of 100 nM AngII in male (n = 5–6 cells per condition, five animals) and female (n = 5 cells per condition, six animals) pial, parenchymal, and mesenteric myocytes. *, P < 0.05; **, P < 0.01.

I_{TRPV4} detected in male and female pial, parenchymal, and mesenteric myocytes. TRPV4 channel activity was determined by recording TRPV4 sparklets using TIRF microscopy, as described previously (Navedo et al., 2006; Nystoriak et al., 2013; Mercado et al., 2014; Zhao et al., 2014; Fig. 2). An advantage of recording TRPV4 sparklets using TIRF microscopy is that it allows the activity of individual channels from a relatively large membrane area to be recorded, thus enabling the identification of discrete sarcolemmal signaling microdomains.

$Ca_V1.2$ channels can also produce sparklets in vascular smooth muscle (Navedo et al., 2005, 2007; Amberg et al., 2007), but TRPV4 sparklets can be distinguished from $Ca_V1.2$ sparklets on the basis of their different amplitudes, pharmacology, and voltage dependencies (Mercado et al., 2014). Accordingly, experiments were performed in the presence of thapsigargin (1 µM), to eliminate Ca^{2+} release from the SR, and the dihydropyridine antagonist nifedipine (10 µM), to block $Ca_V1.2$ channels. All experiments were performed in the presence of physiological 2 mM external Ca^{2+} in the bath solution. At this Ca^{2+} concentration, TRPV4 sparklets have an amplitude of ∼50 nM (Mercado et al., 2014), whereas the amplitude of $Ca_V1.2$ sparklets (<18 nM) falls below the detection limit of our system (Navedo et al., 2005; Amberg et al., 2007). Under these experimental conditions, any $Ca_V1.2$ channels not blocked by nifedipine are unlikely to produce a detectable sparklet that could confound interpretation of our data.

Fig. 2 shows representative TIRF images of pial (Fig. 2 A), parenchymal (Fig. 2 B), and mesenteric (Fig. 2 C) myocytes from male and female mice before and after application of the TRPV4 channel agonist GSK1016790A (100 nM; referred to hereafter as GSK). Time courses of $[Ca^{2+}]_i$ at multiple sites in the sarcolemma of these cells, highlighted by green circles, are shown to the right of each image.

Amplitude histograms were generated for all TRPV4 sparklets recorded in each myocyte type from male (Fig. 3 A) and female (Fig. 3 B) mice, and these data were fit to a multi-Gaussian function using a quantal unit of Ca^{2+} influx of 50 nM (corresponding to an $F/F_0 = 1.41 \pm 0.25$). These analyses showed that the amplitudes of elementary TRPV4 sparklets were similar in cells from different arterial beds in both sexes. In contrast, whereas application of 100 nM GSK increased TRPV4 sparklet density and activity in both female and male cells, the GSK-induced increase in TRPV4 sparklet activity in male pial (0.11 ± 0.02) and parenchymal (0.48 ± 0.14) myocytes was ∼1.3-fold (0.09 ± 0.04) and ∼13-fold (0.04 ± 0.01) higher than that in corresponding female myocytes (Fig. 3, C and D). Indeed, as part of this analysis, we grouped nP_s data from female and male cells and found that, on average, TRPV4 sparklet activity in the presence of GSK was higher in male (0.3 ± 0.08) than in female (0.06 ± 0.02) pial and parenchymal myocytes. Consistent with the I_{TRPV4} data, TRPV4 sparklets were not detectable in mesenteric myocytes under any experimental condition in mice of either sex (Fig. 2 C). These data suggest that differences in I_{TRPV4} amplitude among male and female pial, parenchymal, and mesenteric myocytes are likely the result of differences in TRPV4 channel activity and not the amplitude of elementary sparklets.

AngII increases TRPV4 sparklet activity in pial and parenchymal but not in mesenteric myocytes

We investigated whether the effects of AngII (100 nM) on TRPV4 sparklets vary according to the vascular bed

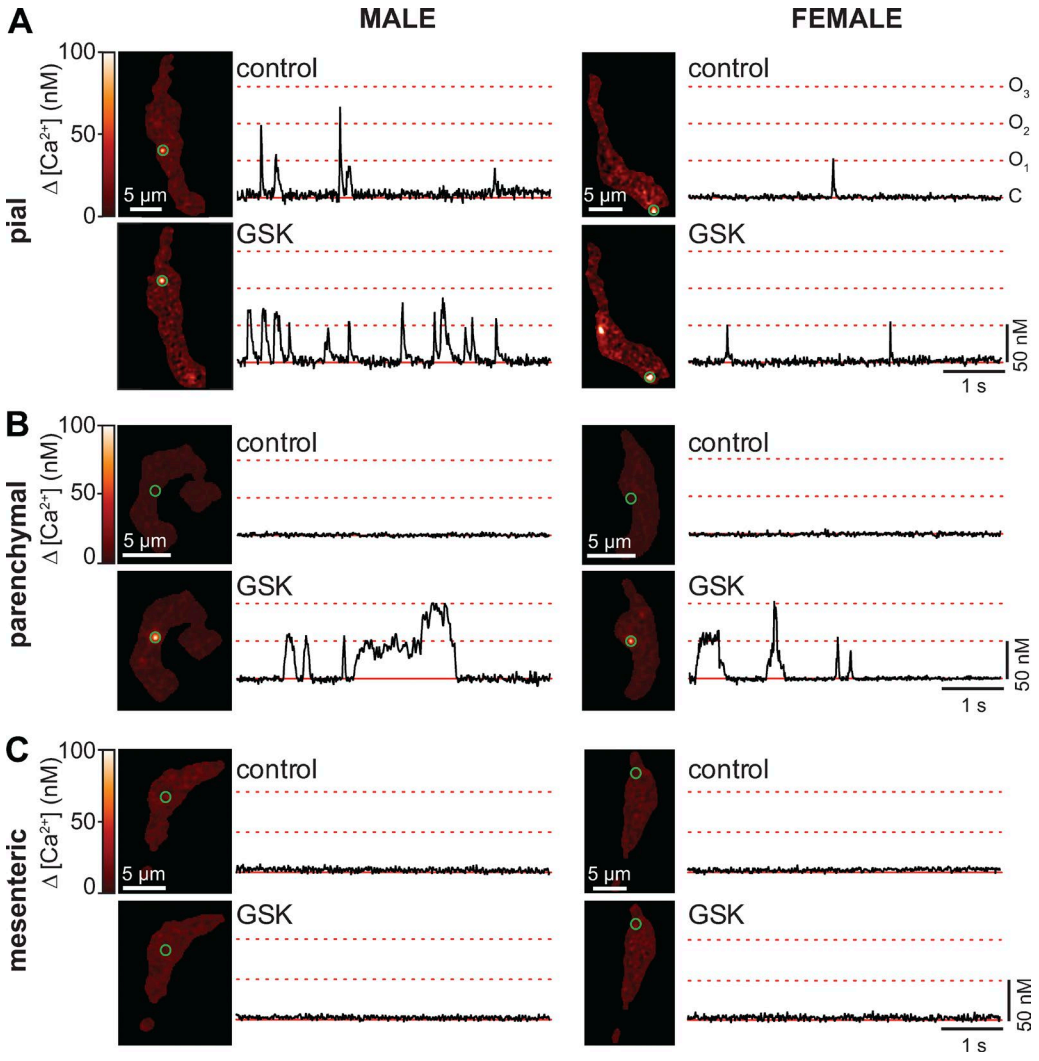

Figure 2. **GSK activates TRPV4 sparklets in pial and parenchymal myocytes, but not in mesenteric myocytes.** (A–C) Set of TIRF images showing representative male (left) and female (right) pial (A), parenchymal (B), and mesenteric (C) myocytes before (control) and after application of the TRPV4 channel agonist GSK (100 nM). Traces to the right of each image show the time course of $[Ca^{2+}]_i$ in regions highlighted by green circles.

and sex of the animal, as was the case for I_{TRPV4} (Fig. 1). TRPV4 sparklets were recorded before and after the application of 100 nM AngII (Fig. 4). Interestingly, we found that AngII increased TRPV4 sparklet activity in myocytes from most, but not all, vascular beds (Fig. 4, A–D). AngII increased TRPV4 sparklet density and activity in pial myocytes (Fig. 4, E and F). Indeed, AngII increased nP_s by ~6.6-fold (from 0.010 ± 0.002 to 0.066 ± 0.014) in pial myocytes from males and by ~2.3-fold (from 0.009 ± 0.002 to 0.021 ± 0.007) in those from females (Fig. 4 E). In parenchymal and mesenteric myocytes, the situation was quite different. Whereas AngII increased TRPV4 sparklet activity ~5-fold (from 0.02 ± 0.02 to 0.09 ± 0.04) in parenchymal myocytes from males, it had no effect on TRPV4 sparklet activity in these myocytes from females. In stark contrast, AngII had no effect on TRPV4 sparklets in either male or female mesenteric myocytes (Fig. 4, E and F). Together with the I_{TRPV4} data, these findings indicate that AngII signaling differentially modulates TRPV4 channel activity throughout the vasculature of male and female mice.

Differential TRPV4 channel and AKAP150 distribution in male and female pial, parenchymal, and mesenteric myocytes

AKAP150 is a scaffold protein that targets signaling proteins to their substrates in the sarcolemma of many cells, including vascular smooth muscle cells. Indeed, we have shown that AKAP150 is required for AngII-induced sparklet activity and TRPV4 regulation in pial myocytes (Navedo et al., 2008; Mercado et al., 2014; Nystoriak et al., 2014). Using GSD super-resolution nanoscopy to investigate the spatial organization of TRPV4 channels and AKAP150, we found that TRPV4

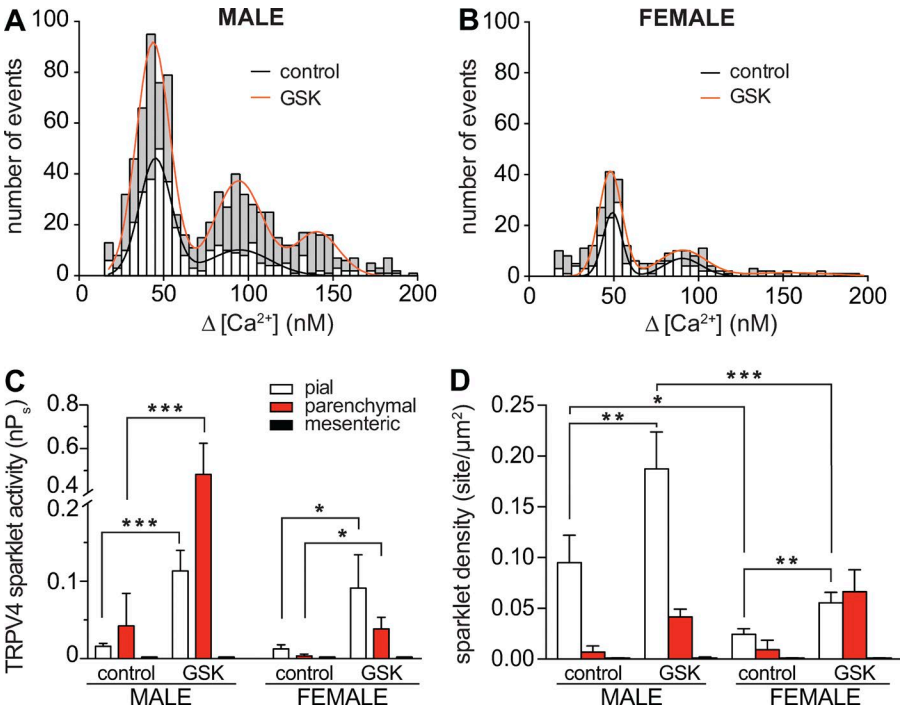

Figure 3. **Sex- and vessel-specific variations in GSK-induced TRPV4 sparklet activity in smooth muscle myocytes.** (A and B) Amplitude histograms of amalgamated TRPV4 sparklets in male (A) and female (B) myocytes (i.e., pial, parenchymal, and mesenteric myocytes) before (white bars) and after 100 nM GSK (gray bars). Black (control) and red (GSK) lines show the best fits of the male and female data using a multi-Gaussian function with a quantal unit of Ca^{2+} influx of 50 nM. (C and D) Bar plots of mean TRPV4 sparklet activity ± SEM (C) and density ± SEM (D) in male (n = 7–8 cells per condition, 12 animals) and female (n = 8–9 cells per condition, 16 animals) pial, parenchymal, and mesenteric myocytes. *, $P < 0.05$; **, $P < 0.01$; ***, $P < 0.001$.

channels and AKAP150 form clusters along the surface membrane of pial (Fig. 5 A), parenchymal (Fig. 5 B), and mesenteric (Fig. 5 C) myocytes.

We determined the area, density, distance, and degree of overlap between TRPV4 and AKAP150 clusters in male and female parenchymal, pial, and mesenteric myocytes. These data are summarized in Table 1. In pial myocytes, the area of AKAP150 clusters was larger in females than in males. This sex-specific difference in area was reversed for TRPV4 clusters, which were larger in male than female pial myocytes. The density of TRPV4 clusters was also higher in male than female pial myocytes. AKAP150 cluster density was similarly higher in male than in female pial myocytes. In control experiments, we found that TRPV4 cluster size was similar in nonpermeabilized and permeabilized cells exposed to a TRPV4 antibody that binds to the extracellular side (Fig. S3). These findings rule out the possibility that TRPV4 clustering is an artifact of cellular permeabilization.

We tested the hypothesis that the distribution of AKAP150 or TRPV4 clusters in the sarcolemma of male and female parenchymal, pial, and mesenteric myocytes was random. To do this, we performed a nearest neighbor analysis of TRPV4 or AKAP150 clusters in all cells and compared the calculated mean nearest neighbor distance and the associated variance to the theoretical values for an object with a distribution that followed a Poisson distribution. This analysis indicated there was not a significant difference ($P > 0.05$) between the spatial distribution of AKAP150 and TRPV4 clusters and the predicted Poisson distribution in male and female parenchymal, pial, mesenteric myocytes. This suggests that the spatial distribution of AKAP150 and TRPV4 clusters in vascular smooth muscle is stochastic.

We also performed a nearest neighbor analysis to determine the distance between AKAP150 and TRPV4 clusters. This analysis suggested that, on average, AKAP150 and TRPV4 clusters were closer together in male than in female pial myocytes (Fig. 5 D and Fig. S5). Moreover, 12 ± 1% of clusters completely overlapped in males, whereas only 6 ± 2% overlapped in females.

We also detected differences in the organization and distribution of AKAP150 and TRPV4 in parenchymal myocytes (Table 1). However, in this vascular bed, male AKAP150 cluster area and TRPV4 cluster area were larger than those in females. The density of AKAP150 clusters was also larger in parenchymal myocytes from males than females, whereas the TRPV4 cluster density in myocytes from this vascular bed was similar in males and females. As was the case for pial myocytes, AKAP150 and TRPV4 clusters were further apart in female than in male parenchymal myocytes (Fig. 5 D and Fig. S5). Indeed, 5 ± 1% of TRPV4 and AKAP150 clusters overlapped in parenchymal myocytes from males, whereas only 1 ± 0.3% overlapped in those from females.

In mesenteric myocytes, the area of AKAP150 clusters was comparable in males and females ($P > 0.05$; Table 1), but the area of TRPV4 clusters was larger in male than in female myocytes. Similar to results obtained in pial and parenchymal myocytes, AKAP150 and TRPV4 clusters were further apart in female than in male mesenteric myocytes ($P > 0.05$; Fig. 5 D and Fig. S5). Whereas 1.0 ± 0.2% of AKAP150 and TRPV4 clusters overlapped in

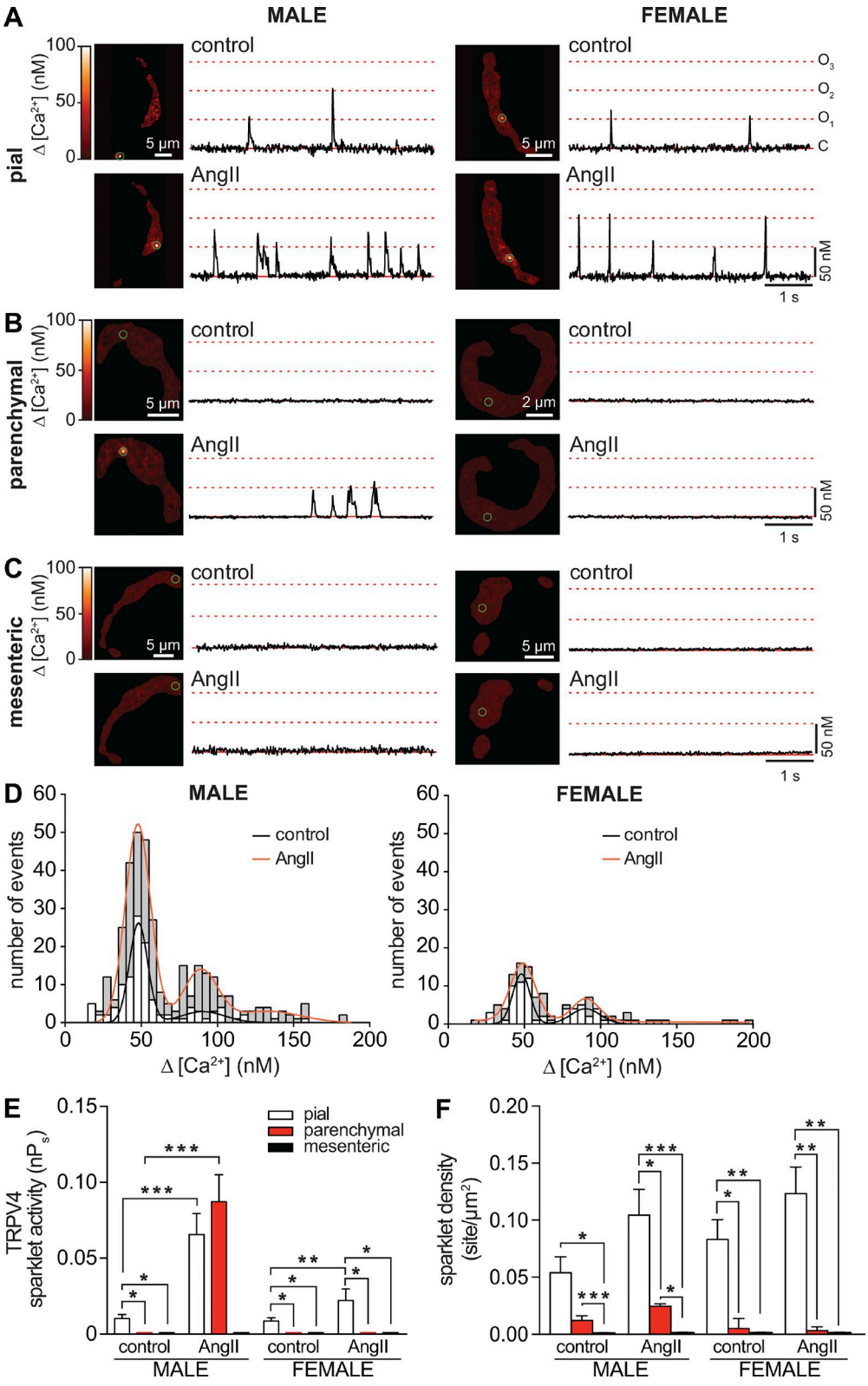

Figure 4. **AngII effects on TRPV4 sparklet activity in smooth muscle depend on sex and vascular bed.** (A–C) TIRF images of representative male (left) and female (right) pial (A), parenchymal (B), and mesenteric (C) myocytes in the absence (control) and presence of 100 nM AngII. Traces to the right of each image show the time course of $[Ca^{2+}]_i$ in regions highlighted by green circles. (D) Amplitude histograms of amalgamated TRPV4 sparklets in male (left) and female (right) myocytes (i.e., pial, parenchymal, and mesenteric myocytes) before (white bars) and after 100 nM AngII (gray bars). Black (control) and red (AngII) lines show the best fits of the male and female data with a multi-Gaussian function with a quantal unit of Ca^{2+} influx of 50 nM.

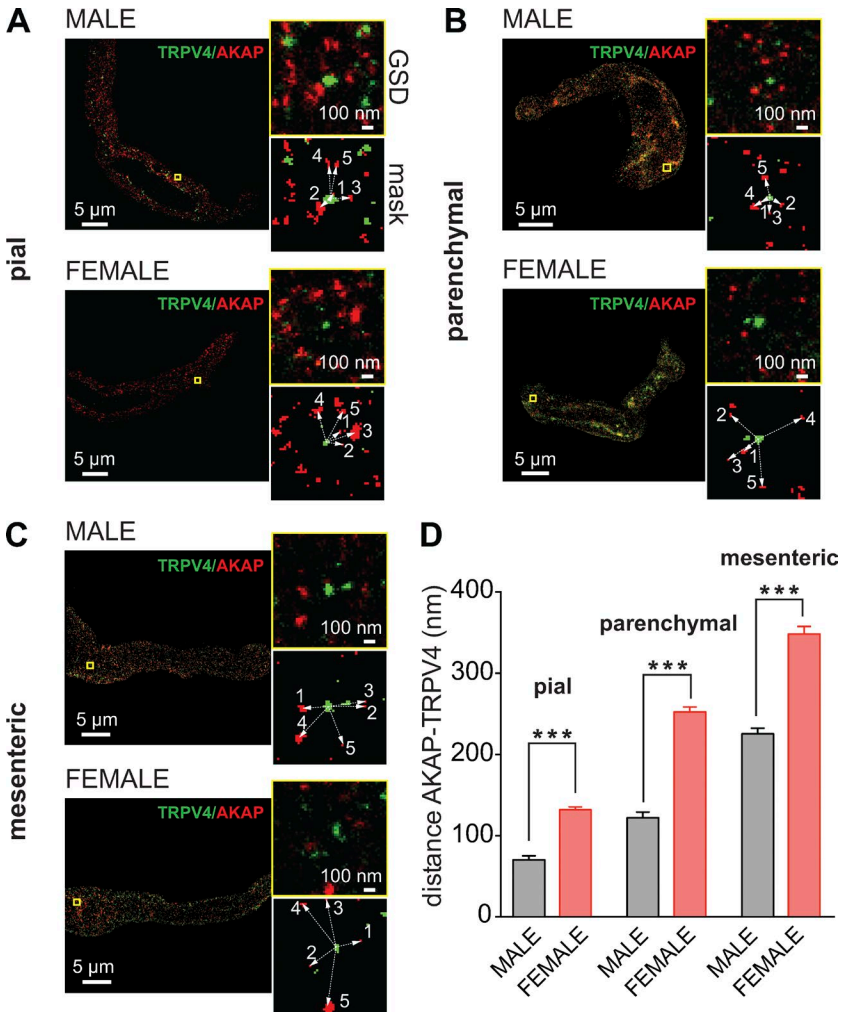

Figure 5. **Differential TRPV4 channel and AKAP150 distribution in male and female mesenteric, pial, and parenchymal myocytes.** (A–C) Super-resolution images of TRPV4 (green) and AKAP150 (red) in pial (A), parenchymal (B), and mesenteric (C) myocytes. Smaller images to the right of each image show expanded views of the regions of interest (ROIs) marked by yellow squares as well as the binary version of the same ROIs (mask). Binary images were used to measure the cluster area and distance to nearest neighbor. (D) Bar plot of the mean distance ± SEM between TRPV4 and AKAP150 clusters in male (n = 750 ROIs from five cells per vascular bed) and female (n = 750 ROIs from five cells per vascular bed). ***, $P < 0.001$.

male mesenteric myocytes, only 0.4 ± 0.2% overlapped in these myocytes from females ($P > 0.05$).

Collectively, these super-resolution data suggest that the size and separation of AKAP150 and TRPV4 clusters in smooth muscle myocytes differs according to sex and vascular bed. Notably, our data suggest a gradation in the separation between AKAP150 and TRPV4 clusters in parenchymal, pial, and mesenteric myocytes. An analysis of the amalgamated data (Fig. 5 D) suggests that the distance between AKAP150 and TRPV4 clusters in smooth muscle myocytes from different vessels followed the rank order, female mesenteric > female parenchymal > male mesenteric > female pial > male parenchymal > male pial.

Differential TRPV4 channel and AKAP150 protein expression in male and female pial, parenchymal, and mesenteric myocytes

TRPV4 and AKAP150 protein levels in parenchymal, pial and mesenteric arteries were analyzed using Western blot analysis (Fig. S4). AKAP150 and TRPV4 protein was largest in male pial myocytes and lowest in male mesenteric myocytes. We generated plots of AKAP150 or TRPV4 cluster density versus protein expression in the same vessel type. This analysis suggested that there is a linear relationship between TRPV4 and AKAP150 expression and cluster density. Thus, AKAP150 or TRPV4 cluster density data are a valid indicator for protein expression in these cells.

(E and F) Bar plot of mean TRPV4 sparklet activity ± SEM (E) and density ± SEM (F) in male (n = 6–7 cells per condition, 11 animals) and female (n = 8–9 cells per condition, 15 animals) pial, parenchymal, and mesenteric myocytes. *, $P < 0.05$; **, $P < 0.01$; ***, $P < 0.001$.

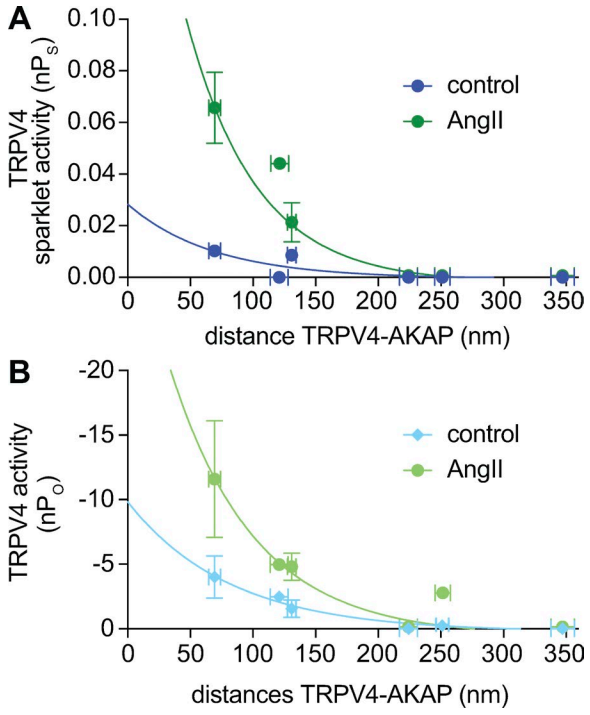

Figure 6. **TRPV4 channel activity depends on its proximity to AKAP150 in arterial myocytes.** (A and B) Mean TRPV4 sparklet ± SEM (nP_s; A) and channel ± SEM (nP_o; B) activity were plotted against the mean nearest edge to edge distance calculated from super-resolution maps using a nearest neighbor analysis. Solid lines show fits to the data using a single-exponential function.

The activity of TRPV4 channels decays as their distance from AKAP150 increases

Having determined the distribution and location of AKAP150 and TRPV4 clusters with nanometer resolution, we examined the relationship between TRPV4 activity and the intermolecular AKAP150–TRPV4 distance in male and female pial, parenchymal, and mesenteric myocytes. To accomplish this, we generated a plot of the mean TRPV4 sparklet (nP_s) and channel (nP_o) activity in each cell as a function of the mean distance separating AKAP150 and TRPV4 clusters in the same cell type (Fig. 6, A and B). We calculated nP_o by dividing I_{TRPV4} at −80 mV by the amplitude of the elementary TRPV4 current recorded under similar experimental conditions (approximately −3.7 pA at −80 mV; Mercado et al., 2014). This analysis provides two related, but independently obtained, measurements of TRPV4 channel activity in arterial myocytes. Accordingly, distance (Table 1), nP_o (Fig. 1), and nP_s (Figs. 3 and 4) values were obtained in separate experiments from male and female parenchymal, pial, and mesenteric myocytes.

Notably, TRPV4 channel activity decreased as the distance from AKAP150 to TRPV4 sparklet sites increased under basal conditions or in the presence of AngII. Data for basal and AngII-induced TRPV4 activity (i.e., nP_s and nP_o) could be fit with single-exponential functions. The decay constants (τ) used to fit nP_s and nP_o values under control conditions and in the presence of AngII were 74 and 127 nm, respectively. Interestingly, this analysis indicated that basal and AngII-induced TRPV4 sparklet activity is undetectably low when the distance between AKAP150 and TRPV4 channels is >200 nm, regardless of the sex of the animal.

The distribution of AKAP150 is dynamic rather than static, particularly during AngII signaling (Mercado et al., 2014; Sonkusare et al., 2014). Indeed, we found that chronic AngII infusion altered this intermolecular distance in pial and parenchymal myocytes. In pial myocytes, chronic AngII infusion increased the mean distance between AKAP150 and TRPV4 clusters from 69 ± 5 to 183 ± 6 nm in males and from 131 ± 3 to 202 ± 4 nm in females ($P < 0.05$; Fig. 7 A). This was associated with a decrease in AKAP150 cluster density and transcript expression in male and female pial myocytes (Fig. 7, B and C). TRPV4 cluster density was also lower in AngII than in control male pial myocytes. Interestingly, AngII infusion increased TRPV4 cluster density and transcript levels in female pial arteries. PKCα expression was lower in AngII than in control male and female pial arteries. Together, these data are consistent with the view that chronic AngII infusion increases the distance between TRPV4 and AKAP150 clusters largely by decreasing expression of AKAP150 in male and female pial myocytes.

In parenchymal myocytes, however, chronic AngII treatment exerted opposite effects in males and females. In male parenchymal myocytes, chronic AngII infusion increased the mean distance between AKAP150 and TRPV4 clusters by nearly 100 nm (Fig. 7 A). In contrast, the distance between AKAP150 and TRPV4 decreased from 251 ± 6 to 226 ± 6 nm in female parenchymal myocytes. Notably, in pial and parenchymal myocytes from male and female infused with AngII, AKAP150–TRPV4 distance values fall beyond the threshold for TRPV4 sparklet activation in Fig. 6. Accordingly, we found that acute application of 100 nM AngII failed to induce TRPV4 sparklet activity in male parenchymal myocytes isolated from mice chronically infused with AngII (Fig. 7, D–F).

The activity of TRPV4 channels is limited by the availability of PKCα

To test the hypothesis that TRPV4 channels in male and female mesenteric myocytes are silent because of the limited local availability of PKCα (Figs. 2 C and 4 C), we monitored $[Ca^{2+}]_i$ and I_{TRPV4} in cells dialyzed with an intracellular solution containing activated PKCα (1 U/ml; Fig. 8). In the representative female mesenteric myocyte shown, the vast majority (>95%) of the imaged sarcolemma exhibited sustained elevations in Ca^{2+} influx after ∼5 min from the beginning the experiment (Fig. 8, A and B). Similar results were obtained in seven

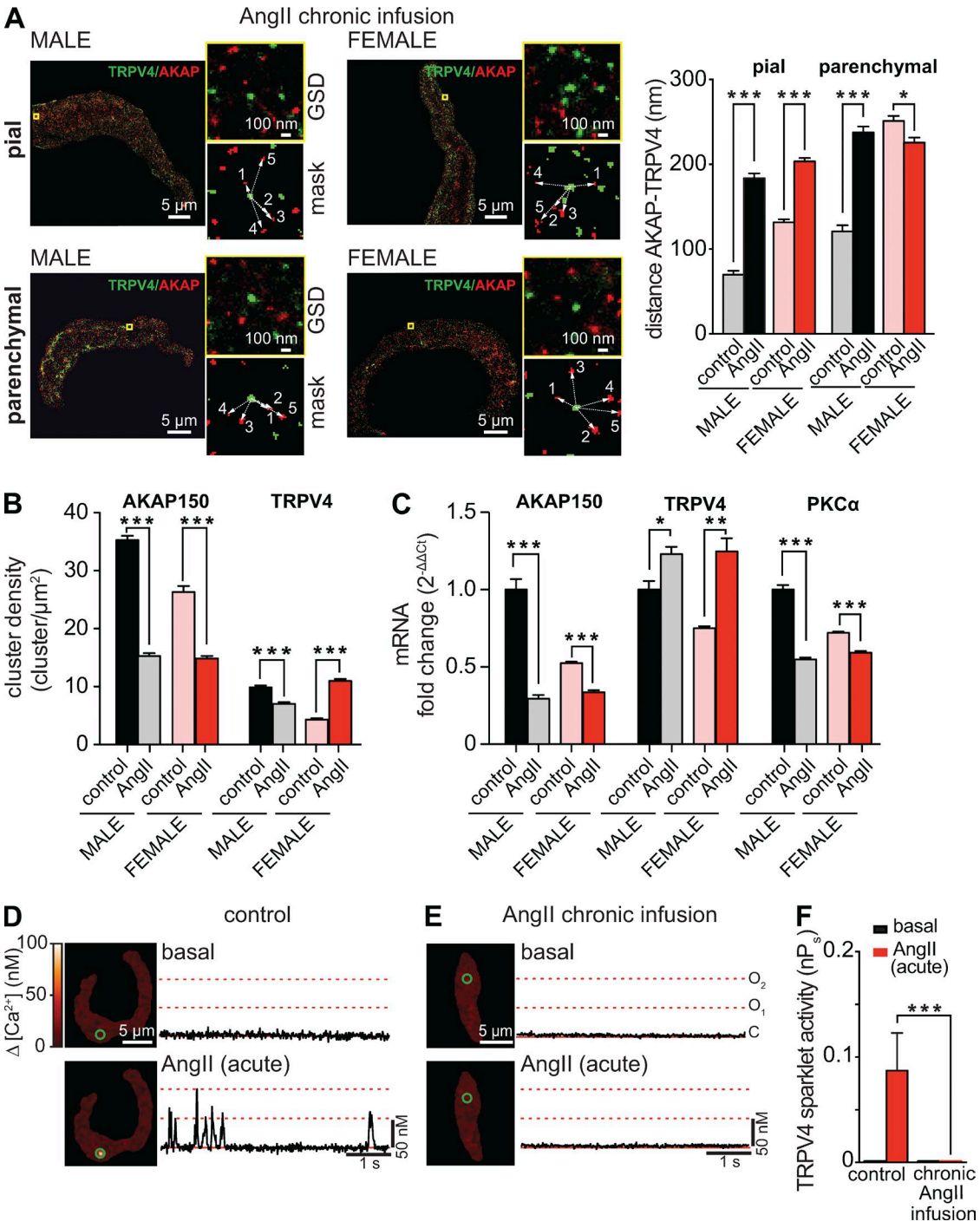

Figure 7. **Chronic infusion of AngII increases AKAP150–TRPV4 distance in pial and parenchymal myocytes.** (A) Two-color super-resolution localization maps of AKAP150 (red) and TRPV4 (green) in male (left) and female (right) pial and parenchymal myocytes from mice infused with AngII for 7 d. To the right, a zoomed-out image of the region of interest (top) and the binary image (mask, bottom) used for nearest neighbor analysis. The bar plot shows the mean ± SEM distance between AKAP150 and TRPV4 clusters in male (n = 1,000 ROIs from five cells per condition) and female (n = 1,000 ROIs from five cells per condition) pial and parenchymal myocytes from control mice (i.e., saline infusion) and mice chronically infused with AngII. (B) Bar plot of the mean ± SEM cluster density for AKAP150 and TRPV4 in pial myocytes from male and female mice infused with saline solution (control) or with AngII. (C) Real-time PCR analysis of the mean ± SEM fold change of mRNA for AKAP150, TRPV4, and PKCα in control and AngII-infused arteries (n = 3). (D and E) TIRF images of male parenchymal myocytes in control conditions and during acute application of 100 nM AngII. The cell in D was isolated from a mouse infused with saline, whereas the cell in E was isolated from a mouse chronically infused with AngII. Traces at right show the time course of $[Ca^{2+}]_i$ in regions highlighted by green circles. (F) The bar plot shows mean ± SEM TRPV4 nP_s values in male parenchymal myocytes (n = 4 cells per treatment, eight animals) from control and AngII-infused mice before and after acute AngII treatment. *, P < 0.05; **, P < 0.01; ***, P < 0.001.

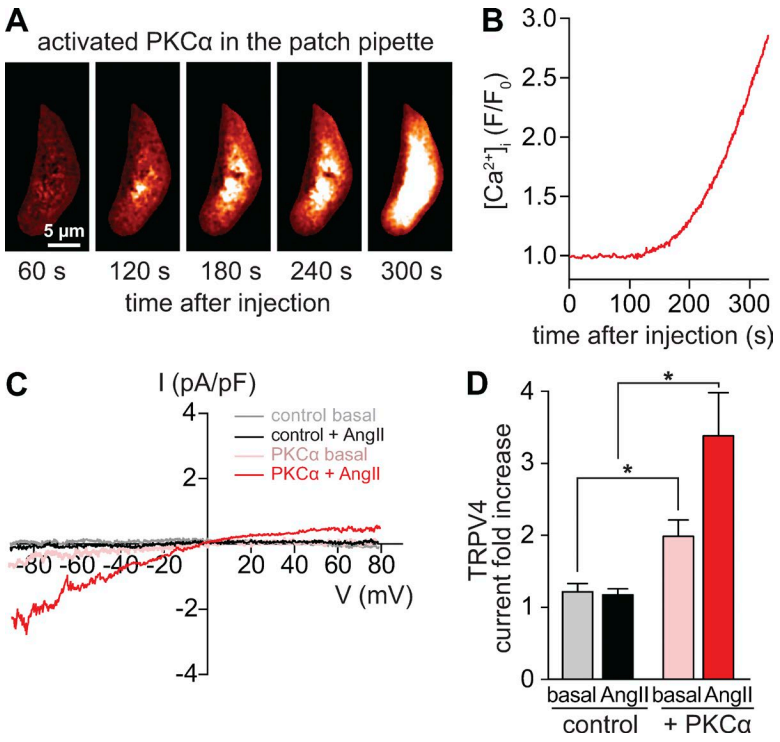

Figure 8. **Increasing PKCα availability evokes TRPV4 channel activity in mesenteric myocytes.** (A) TIRF image of a representative male mesenteric myocyte dialyzed with active PKCα (1 U/ml) recorded 1–5 min after gaining access to the cell interior. (B) Spatially averaged $[Ca^{2+}]_i$ from a myocyte dialyzed with active PKCα in the presence of the L-type $Ca_V1.2$ channel antagonist nifedipine (10 μM). (C) TRPV4 current records obtained using the whole-cell patch-clamp configuration. TRPV4 currents were defined as the fraction of the current sensitive to HC067047 (1 μM; control) and were obtained by subtracting current traces evoked by voltage ramps in the presence of HC067047 from traces in control conditions or in the presence of 100 nM AngII. (D) Bar plot showing mean ± SEM fold increase in I_{TRPV4} at −80 mV in the presence (n = 7 cells) and absence (n = 7 cells) of active PKCα in the pipette solution. *, $P < 0.05$.

independent experiments involving male and female mesenteric myocytes. In sharp contrast, the maximum fraction of the imaged membrane undergoing persistent Ca^{2+} influx in control cells was always small (1–5%).

In agreement with the data in Fig. 1, we could not detect I_{TRPV4} in control mesenteric myocytes (i.e., without activated PKCα) before or after AngII application (Fig. 8 C). However, consistent with the $[Ca^{2+}]_i$ data in Fig. 8, A and B, internal perfusion with activated PKCα induced an I_{TRPV4} that increased nearly threefold in response to AngII (Fig. 8 D). This increase in I_{TRPV4} is likely produced by an AngII-induced increase in PKCα activity in response to higher DAG and local Ca^{2+} levels in the cell. Collectively, these data suggest that although functional TRPV4 channels are broadly expressed in the surface membrane of mesenteric myocytes, the location and number of such sites that exhibit active Ca^{2+} influx are limited by the availability of PKCα. Taken together with data establishing a minimum effective distance between TRPV4 and PKC-associated AKAP150 clusters (Fig. 6), these findings further support the general conclusion that TRPV4 sparklet activity in smooth muscle myocytes is limited by the spatial distribution of PKCα.

An in silico analysis shows that TRPV4 channel activity depends on its proximity to AKAP150 clusters

We built a computational model to perform an in silico analysis of AKAP150 distribution, PKCα activity, and TRPV4 channel activity. The model incorporates the cluster area and densities generated using super-resolution nanoscopy (Table 1). The model assumes random distribution of AKAP150 and TRPV4 clusters in all cells. This assumption is reasonable, as analysis of super-resolution images from male and female pial, parenchymal, and mesenteric myocytes revealed that the location of AKAP150 and TRPV4 clusters follows a Poisson distribution.

Fig. 9 A shows six two-dimensional images of simulated TRPV4 (green) and AKAP150 (red) clusters. The areas and densities of these clusters are similar to those measured using super-resolution nanoscopy of pial, parenchymal, and mesenteric myocytes (Table 1). The distance between in silico clusters is similar to those measured in cells (Fig. 9 B). Using these data, we proceeded to generate three-dimensional model for TRPV4 channel activity in male and female pial, parenchymal, and mesenteric myocytes. The model assumes that under basal conditions (i.e., low PKCα activity), there is one active PKCα per AKAP150 cluster in simulated male and female pial, parenchymal, and mesenteric myocytes. The active PKCα detaches from AKAP150 and randomly walks near the sarcolemma. The model also assumes that a collision between a PKCα and a TRPV4 channel will result in the opening of the channel.

The model uses the diffusion coefficient (D) and time constant of the activated state (τ_{PKC}) to simulate the range and duration of PKCα mobility. The diffusion coefficient for activated Ca^{2+}/DAG-sensitive PKCα in hippocampal neurons is 0.33 $\mu m^2/s$ (Craske et al., 2005). Our sparklet and super-resolution data provide a means for estimating τ_{PKC}. For a two-dimensional diffusional process, the mean distance that the signaling protein travels $(r) = (2 \times D \times \tau_{PKC})^{1/2}$, where r is the distance at which 63% of PKCα will be inactive (Teruel

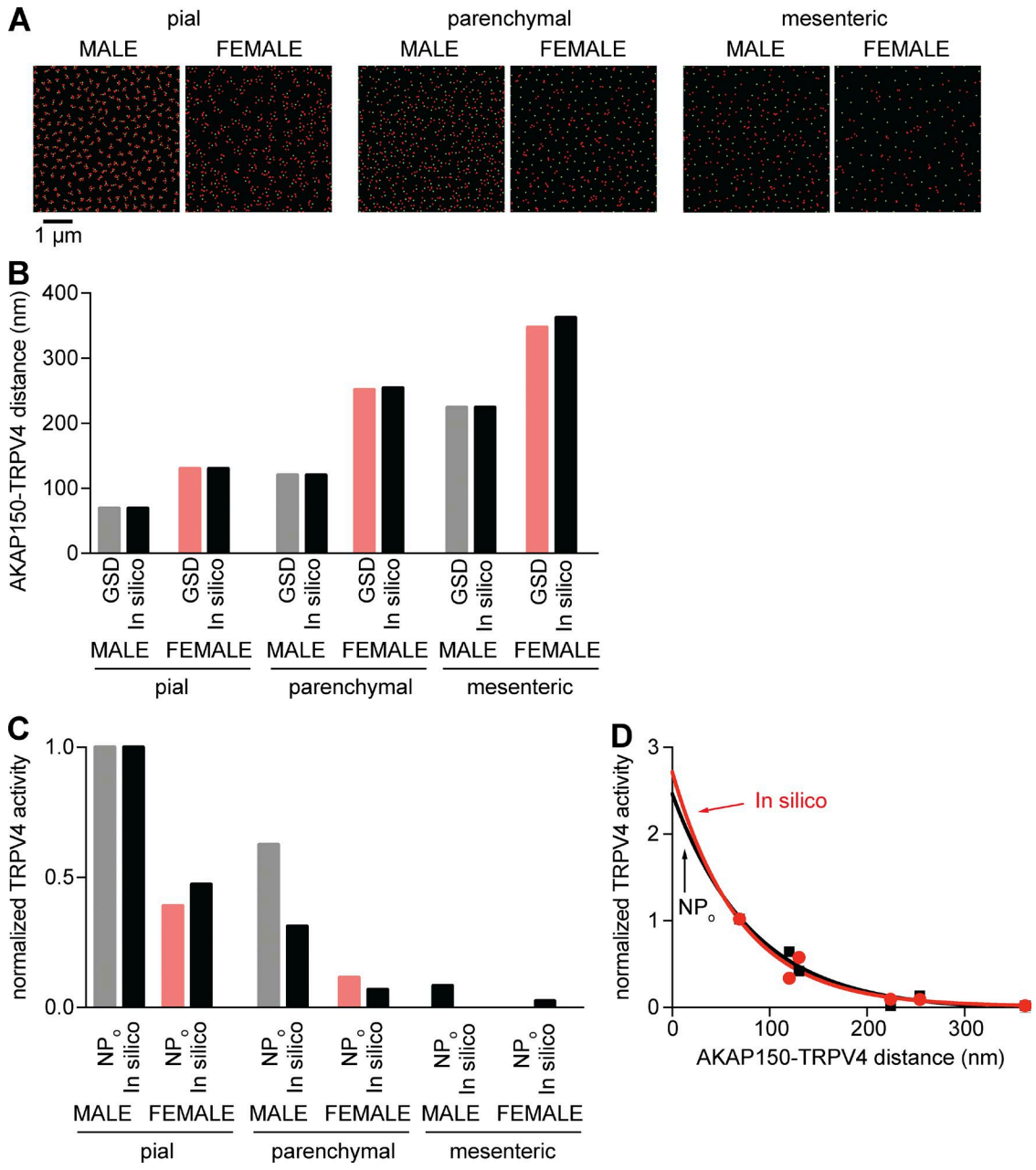

Figure 9. **In silico analysis suggests that TRPV4 channel activity depends on its proximity to AKAP150.** (A) Simulated images of randomly distributed TRPV4 (green) and AKAP150 (red) clusters in male and female pial (left), parenchymal (center), and mesenteric (right) myocytes. (B) Bar plot of the in vitro (measured using GSD super-resolution nanoscopy) and in silico distances between AKAP150 and TRPV4 clusters. (C) Experimentally determined (i.e., nP_o) and in silico calculated TRPV4 channel activities. (D) Plot of in vitro (nP_o; black squares and line) and in silico (red circle and line) TRPV4 channel versus the mean AKAP150 to TRPV4 distance. Solid lines show fits to the data using a single-exponential function.

and Meyer, 2000). Our data suggest that r is ~74 nm under basal conditions. Solving this equation for τ_{PKC} (assuming that PKCα has a similar diffusion coefficient in neurons and smooth muscle cells) yields a τ_{PKC} value of 8 ms under control conditions. The model uses these D and τ_{PKC} values. To provide a visual representation of how our model works, we created videos of simulations of PKCα diffusion and TRPV4 sparklets using these D and τ_{PKC} values as well as the areas and densities of these clusters of male and female pial, parenchymal, and mesenteric myocytes (Videos 1, 2, 3, 4, 5, and 6).

Fig. 9 C shows that in silico and in vitro (i.e., nP_o) values of TRPV4 channel activity are similar. Thus, our model was able to reproduce the observation that TRPV4 channel activity is relatively high when the distance between TRPV4 and AKAP150 clusters is similar to that of male pial myocytes and lowest when it is similar to male and female myocytes. Importantly, our

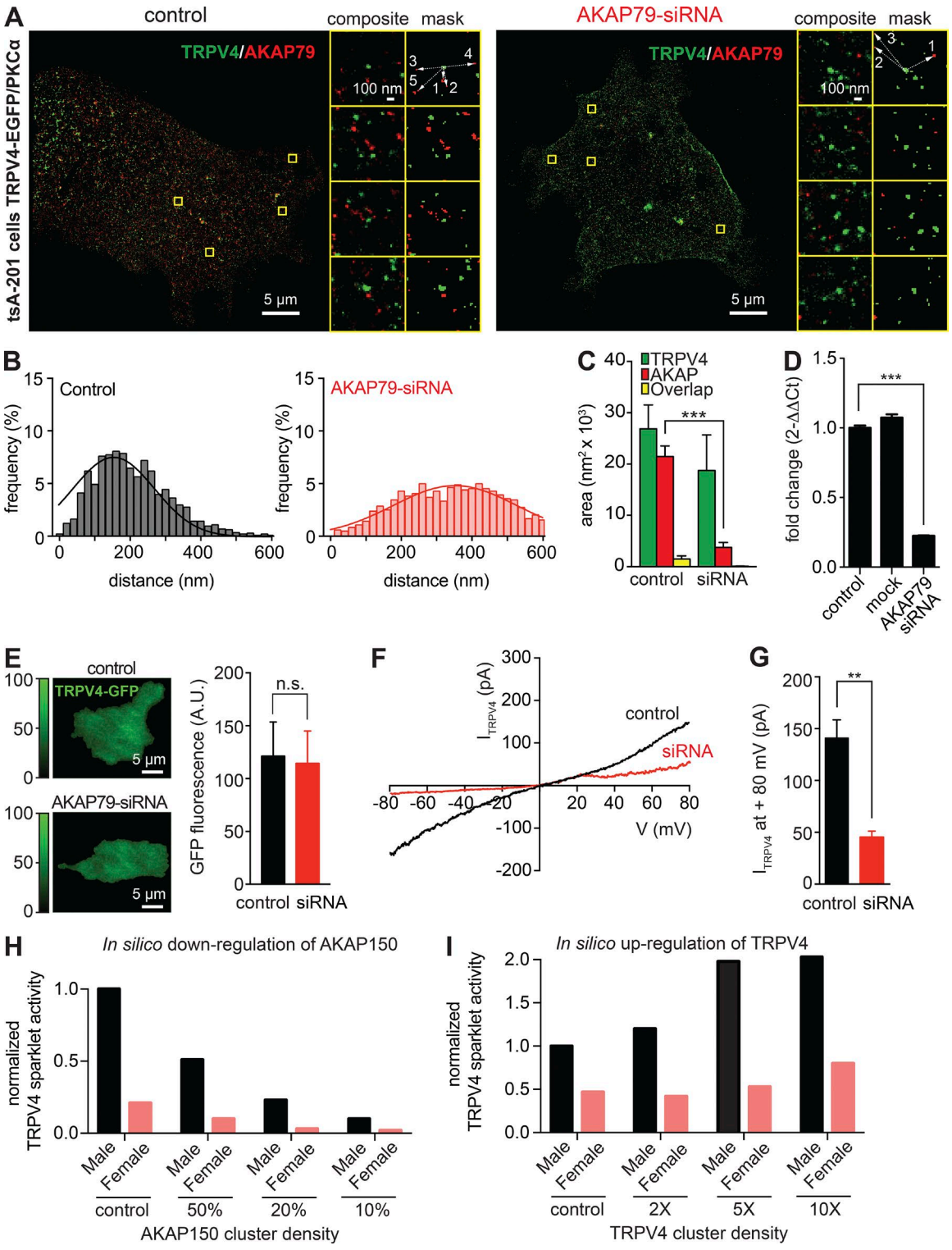

Figure 10. **Effects of the down-regulation of AKAP79 on TRPV4 activity.** (A) Representative two-colored super-resolution images generated using GSD in control tsA-201 cells (left) and AKAP79-siRNA–treated cells (right) stained with anti-AKAP79 and anti-TRPV4 antibodies followed by Alexa Fluor 568– and Alexa Fluor 647–labeled secondary antibodies, respectively. Composite and mask images to the right show the boxed regions at higher zoom. (B) Two histograms representing the frequency of distances between TRPV4 and AKAP70 proteins in control conditions (left, gray) and in AKAP79-siRNA–treated cells (right, red). Solid lines represent best-fit Gaussian distribution. TRPV4-AKAP distance means are 155.3 ± 5.25 nm in control cells and 352.1 ± 7.36 nm in AKAP-siRNA cells. (C) Bar plot showing TRPV4, AKAP79, and overlap mean ± SEM areas (nm^2) in control conditions and under presence of AKAP79-siRNA. (D) Real-time PCR analysis of mean ± SEM diffrence of AKAP79 mRNA in control, mock, and AKAP79-siRNA–treated tsA-201 cells. (E) Representative TIRF images of TRPV4-EGFP in control (top) and AKAP79-siRNA–treated (bottom) tsA-201

model shows that, as in vitro, in silico TRPV4 channel activity decays exponentially as the distance between AKAP150 and TRPV4 clusters increases. The $\tau_{\text{in silico}}$ was 69 nm, which is close to the experimentally determined τ for nP_o and nP_s (i.e., 74 nm; Fig. 9 D).

We simulated the effects of a 10-fold increase in the number of active PKCα per AKAP150 cluster in all myocytes. The model predicted an increase in TRPV4 activity in all cell types. However, consistent with our in vitro data, TRPV4 sparklet activity was predicted to follow the same order as under control conditions. That is, TRPV4 sparklet activity is highest in male pial myocytes and lowest in female mesenteric myocytes. Indeed, under basal (i.e., 1 active PKCα per AKAP150 cluster) and high PKCα activity (i.e., 10 active PKCα per AKAP150 cluster) conditions, TRPV4 channel activity in female mesenteric myocytes was only 0.7% and 0.9% that of male pial myocytes, respectively.

In vitro and in silico down-regulation of AKAP79/150 cluster density decreases TRPV4 channel activity

We tested the hypothesis that an increase in the distance between AKAP150 and TRPV4 cluster is sufficient to decrease TRPV4 channel activity. To do this, we used tsA-201 cells transfected with EGFP-tagged TRPV4 channels. These cells have endogenous AKAP79, the human orthologue of rodent AKAP150. We performed super-resolution imaging and recorded I_{TRPV4} in control cells and in tsA-201 cells treated with a siRNA against AKAP79 (Fig. 10). Treatment with this siRNA decreased AKAP79 expression by 80 ± 5%. The mean distance between AKAP79 and TRPV4 clusters increased from 155 ± 5 to 352 ± 7 nm in control and siRNA-treated cells. Consistent with our hypothesis, the magnitude of basal (i.e., unstimulated) TRPV4 currents (at +80 mV) were about threefold smaller in control (141 ± 18 pA) and siRNA-treated cells (45 ± 6 pA), even though TRPV4 expression (assessed by measuring EGFP fluorescence) was similar in control and siRNA-treated cells. These findings suggest that AKAP79 targets PKCα to the surface membrane of tsA-201 cells and that basal activity of the kinase is sufficient to elevate TRPV4 activity in these cells.

Finally, we used our mathematical model to perform an in silico test of the effects of 2-, 5-, and 10-fold changes in AKAP150 or TRPV4 expression (i.e., cluster density) on TRPV4 channel activity in female and male mesenteric myocytes. Consistent with the tsA-201 experiments shown in Fig. 10, a decrease in AKAP150 cluster density was, by itself, sufficient to reduce TRPV4 sparklet activity in a simulated male and female mesenteric myocyte (Fig. 10 H). Furthermore, the model predicted that increasing TRPV4 expression is sufficient to induce higher PKCα-driven TRPV4 channel activity in mesenteric myocytes (Fig. 10 I). Notably, increasing TRPV4 expression translated into larger in silico increases of TRPV4 sparklet activity in male than in female myocytes. For example, a fivefold increase in TRPV4 expression predicted a ≈2-fold increase in sparklet activity in male but only a ≈1.1-fold increase in female myocytes.

DISCUSSION

In this study, we provide a quantitative analysis of the relationship between the localization and activity of TRPV4 channels in male and female arterial and arteriolar myocytes. We found that basal and AngII-induced TRPV4 channel activity decays exponentially as the distance between TRPV4 and PKCα-associated AKAP150 clusters increases in different vessels from male and female mice. A key finding is that TRPV4 sparklet activity falls to undetectable levels if the mean distance between these clusters is greater than 200 nm. An important implication of our findings is that by determining the distance between TRPV4 channels and AKAP150 using super-resolution nanoscopy, it is possible to make reasonable predictions of TRPV4 channel activity in smooth muscle, even without applying patch-clamp or imaging approaches.

Our in vitro and in silico findings add quantitative information to a structural model that has been proposed to explain heterogeneous TRPV4 channel activity along the surface membrane of endothelial cells and arterial and arteriolar myocytes (Fig. 11; Mercado et al., 2014; Sonkusare et al., 2014). According to this model, the anchoring protein AKAP150 plays a central role in forming a macromolecular signaling complex that regulates TRPV4 channels, and hence TRPV4 sparklet activity, in vascular smooth muscle by targeting PKCα to specific regions of the sarcolemma. In arterial myocytes, PKCα is activated by an increase in local $[Ca^{2+}]_i$ (e.g., $Ca_V1.2$ sparklet, TRPV4 sparklet, or ryanodine receptor-mediated Ca^{2+} spark) and DAG produced by the activation of G_q protein–coupled receptors, including AngII receptors. Biochemical and cell-based studies have suggested a potential mechanism for local Ca^{2+}-dependent activation of PKCα (Hoshi et al., 2010), proposing that as Ca^{2+} enters the cell, it recruits Ca^{2+}/calmodulin to a PKCα-containing

cells. Bar plot of mean ± SEM TRPV4-EGFP fluorescence in control and AKAP79-siRNA–treated tsA-201 cells (right). A.U., arbitrary units. (F) Representative I_{TRPV4} records from a control and AKAP79-siRNA–treated cell. (G) Bar plot of the mean ± SEM amplitude of I_{TRPV4} at 80 mV in control and AKAP79-siRNA–treated cells. (H and I) Mathematical simulation of the effects of down-regulating AKAP150 (H) or up-regulating TRPV4 (I) on TRPV4 channel activity in male and female myocytes. **, P < 0.01; ***, P < 0.001.

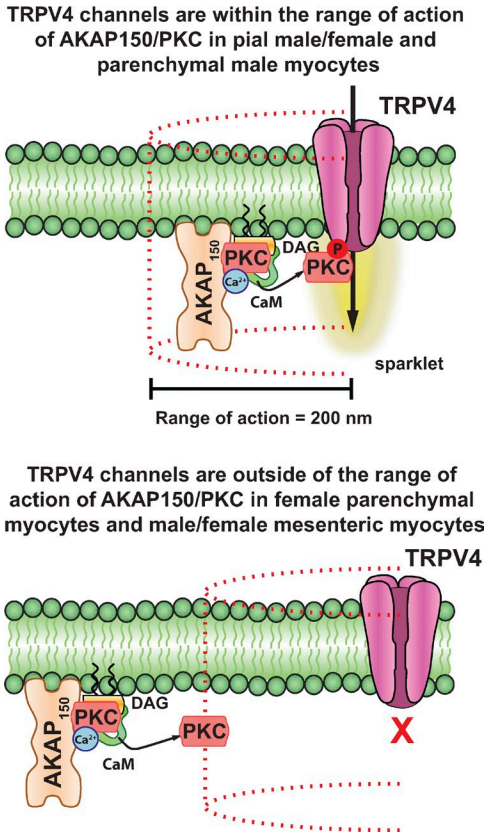

Figure 11. **A model depicting distance constraints on activation of TRPV4 channels by AKAP150-bound PKCα in vascular smooth muscle cells.** Our in vitro and in silico data suggest that in arterial smooth muscle, the radius of action of an activated PKCα is ~200 nm. In male and female pial myocytes as well as male parenchymal myocytes, the level of expression of AKAP150/PKCα complexes is sufficiently high to locate many of these complexes within 200 nm of TRPV4 channels. Accordingly, TRPV4 activity in these cells is relatively high. In cells such as mesenteric myocytes, which express relatively low levels of AKAP150 and/or TRPV4, the density of these proteins in the sarcolemma is low. This results in an increase in the mean distance between AKAP150 and/or TRPV4 clusters. In cells (e.g., female parenchymal myocytes and male and female mesenteric myocytes) where the distance between these clusters is >200 nm, TRPV4 channel activity is undetectably low.

AKAP150 complex, which then releases PKCα, allowing it to initiate a random walk during which it can phosphorylate nearby targets.

Our data suggest that the overall level of TRPV4 sparklet activity is determined by the relative distance of AKAP150-associated PKCα from TRPV4 channel clusters as well as the number of active PKCα molecules, their mobility, and, in principle, their lifetime. Although an increase in the number of active PKCα molecules could increase TRPV4 channel activity, total channel activity is limited by how far the channel is from where the kinase is anchored in the membrane. TRPV4 sparklet activity is at its highest when channels are ≤50 nm away from AKAP150 but becomes undetectably low if clusters of these two proteins is located ~200 nm or more away from each other.

A question prompted by our work is, what determines the distance between AKAP150 and TRPV4 channels in male and female mesenteric, pial, and parenchymal myocytes? Our data are consistent with the view that this is the result of the stochastic distribution of differentially expressed AKAP150 and TRPV4 proteins in the sarcolemma of parenchymal, pial, and mesenteric myocytes. The distance between TRPV4 and AKAP150 clusters is lowest in cells in which the expression of these protein is highest (i.e., male pial myocytes) and highest in cells in which their expression level is lowest (i.e., female mesenteric myocytes). Indeed, in mesenteric myocytes, which express functional TRPV4 channels, the expression of AKAP150/PKCα complexes seems to be a key limiting factor of TRPV4 activity. In these cells, increasing AKAP150 expression is likely a more efficient strategy to increase TRPV4 activity than increasing TRPV4 expression alone. A future study should investigate the role of sex hormones, transcription factors, and microRNA, among other factors, in regulating the expression of AKAP150 and TRPV4 mRNA and protein in parenchymal, pial, and mesenteric myocytes.

A key feature of this model is that AKAP150 and TRPV4 channels are mobile and can interact dynamically. Thus, the distance separating these proteins could change over time depending on physiological conditions. For example, an increase in the expression of TRPV4 and AKAP150 or the size and/or number of their respective clusters could potentially lead to a decrease in the distance between these two proteins. In any case, an interesting prediction of this model is that TRPV4 activity may not be restricted to a small, fixed number of channels. Instead, all TRPV4 channels in the membrane could potentially participate in Ca^{2+} influx, but the specific subset of active TRPV4 channels could change with time depending on the proximity of AKAP150 complexes to these channels and the activity of AKAP150-associated PKCα.

Our study also sheds light on mechanisms of differential smooth muscle function along the arterial tree in both females and males. We detected clear differences in the activity of TRPV4 channels among vessels according to biological sex. Indeed, on average, the distance between TRPV4 channels and AKAP150, as well as TRPV4 sparklet activity, was higher in male than in female myocytes. Because TRPV4 channels oppose myogenic tone during AngII signaling, the expectation is that the role of TRPV4 channels in opposing vasoconstriction will likely vary among vessels and between sexes. An analysis of our amalgamated data suggests that the ability of TRPV4 function to oppose AngII vasoconstriction is lowest in female mesenteric myocytes and highest in male pial myocytes. Future experiments will be required to confirm this generalization.

An intriguing finding of this study is that although mesenteric myocytes express functional TRPV4 channels, their activity is extremely low in these cells. Although our data show that TRPV4 channels are unresponsive to the agonists GSK and AngII in mesenteric myocytes, it would be interesting to investigate whether they can be activated by 11,12-EET, as Earley and colleagues (Earley et al., 2005, 2009) previously demonstrated occurs in pial myocytes. A difference in how TRPV4 channels in pial, parenchymal, and mesenteric myocytes respond to AngII and 11,12-EET could reflect different regulatory mechanisms of these channels as well as distinct physiological roles that could be necessary to support responses to specific physiological demands within each vascular bed.

Arterial smooth muscle depolarization and increased myogenic tone are hallmarks of hypertension. Our work provides insights into the mechanisms underlying smooth muscle dysfunction during this pathological condition. Chronic activation AngII signaling has been shown to elevate mean arterial pressure and decrease expression of the accessory β1 subunit of BK channels. Loss of β1 decreases the Ca^{2+} sensitivity and thus makes BK channels less likely to be activated by Ca^{2+} release via ryanodine receptors (i.e., Ca^{2+} sparks) in arterial myocytes (Amberg et al., 2003; Nieves-Cintrón et al., 2007, 2008). Here, we show that sustained elevations in AngII are associated with a decrease in TRPV4 function under basal conditions as well as in response to acute activation of AngII receptors. Our data suggest that this happens because sustained AngII signaling activation down-regulates AKAP150 and/or TRPV4, increasing the distance in the membrane between these two proteins. However, chronic activation of AngII receptors has also been shown to induce desensitization and internalization of these receptors (Sasamura et al., 1994; Oppermann et al., 1996; Ishizaka et al., 1997). Thus, a combination of lower TRPV4 activity (because of longer intermolecular distances between these channels and AKAP150/PKCα complexes), AngII receptor desensitization, as well as lower β1 subunit expression are likely to lead to lower BK channel activity and thus to increased depolarization of arterial myocytes during hypertension. Membrane depolarization increases myogenic tone by increasing the opening probability of $Ca_V1.2$ channels, which elevates $[Ca^{2+}]_i$, and triggers contraction.

In conclusion, we propose that PKCα/AKAP150 and TRPV4 channels form dynamic signaling domains that control TRPV4 activity in arterial myocytes (Fig. 11). Activation of G_q-coupled AngII receptors enhances TRPV4 sparklet activity through activation of AKAP150-associated PKCα located near these channels. For optimal signaling, AKAP150 and TRPV4 channel clusters must be located within ∼50 nm (or closer) of each other. If this distance exceeds 200 nm, TRPV4 channels are rendered incapable of responding to activation of AKAP150-associated PKCα. Because the relative distance between TRPV4 and AKAP150 is also an important determinant of TRPV4 sparklet activity in endothelial cells (Sonkusare et al., 2014), and perhaps other cells, our findings have broad implications in vascular and other cell types.

ACKNOWLEDGMENTS

We thank Ms. Dellaney Rudolph-Gandy for technical support.

Support for this work was provided by National Institutes of Health grants HL085870, HL098200, and HL121706. S. O'Dwyer was supported by a Pharmacology Training Program funded by the National Institute of General Medical Sciences (T32GM099608).

The authors declare no competing financial interests.

Angus C. Nairn served as editor.

Submitted: 6 October 2016
Revised: 3 March 2017
Accepted: 27 April 2017

REFERENCES

Amberg, G.C., A.D. Bonev, C.F. Rossow, M.T. Nelson, and L.F. Santana. 2003. Modulation of the molecular composition of large conductance, Ca^{2+} activated K^+ channels in vascular smooth muscle during hypertension. *J. Clin. Invest.* 112:717–724. http://dx.doi.org/10.1172/JCI200318684

Amberg, G.C., M.F. Navedo, M. Nieves-Cintrón, J.D. Molkentin, and L.F. Santana. 2007. Calcium sparklets regulate local and global calcium in murine arterial smooth muscle. *J. Physiol.* 579:187–201. http://dx.doi.org/10.1113/jphysiol.2006.124420

Bayliss, W.M. 1902. On the local reactions of the arterial wall to changes of internal pressure. *J. Physiol.* 28:220–231. http://dx.doi.org/10.1113/jphysiol.1902.sp000911

Chrissobolis, S., and F.M. Faraci. 2010. Sex differences in protection against angiotensin II-induced endothelial dysfunction by manganese superoxide dismutase in the cerebral circulation. *Hypertension.* 55:905–910. http://dx.doi.org/10.1161/HYPERTENSIONAHA.109.147041

Craske, M.L., M. Fivaz, N.N. Batada, and T. Meyer. 2005. Spines and neurite branches function as geometric attractors that enhance protein kinase C action. *J. Cell Biol.* 170:1147–1158. http://dx.doi.org/10.1083/jcb.200503118

Dempsey, G.T., J.C. Vaughan, K.H. Chen, M. Bates, and X. Zhuang. 2011. Evaluation of fluorophores for optimal performance in localization-based super-resolution imaging. *Nat. Methods.* 8:1027–1036. http://dx.doi.org/10.1038/nmeth.1768

Earley, S., B.J. Waldron, and J.E. Brayden. 2004. Critical role for transient receptor potential channel TRPM4 in myogenic constriction of cerebral arteries. *Circ. Res.* 95:922–929. http://dx.doi.org/10.1161/01.RES.0000147311.54833.03

Earley, S., T.J. Heppner, M.T. Nelson, and J.E. Brayden. 2005. TRPV4 forms a novel Ca^{2+} signaling complex with ryanodine receptors and BK_{Ca} channels. *Circ. Res.* 97:1270–1279. http://dx.doi.org/10.1161/01.RES.0000194321.60300.d6

Earley, S., T. Pauyo, R. Drapp, M.J. Tavares, W. Liedtke, and J.E. Brayden. 2009. TRPV4-dependent dilation of peripheral resistance arteries influences arterial pressure. *Am. J. Physiol. Heart Circ. Physiol.* 297:H1096–H1102. http://dx.doi.org/10.1152/ajpheart.00241.2009

Everaerts, W., X. Zhen, D. Ghosh, J. Vriens, T. Gevaert, J.P. Gilbert, N.J. Hayward, C.R. McNamara, F. Xue, M.M. Moran, et al. 2010.

Inhibition of the cation channel TRPV4 improves bladder function in mice and rats with cyclophosphamide-induced cystitis. *Proc. Natl. Acad. Sci. USA.* 107:19084–19089. http://dx.doi.org/10.1073/pnas.1005333107

Fan, H.C., X. Zhang, and P.A. McNaughton. 2009. Activation of the TRPV4 ion channel is enhanced by phosphorylation. *J. Biol. Chem.* 284:27884–27891. http://dx.doi.org/10.1074/jbc.M109.028803

Fleischmann, B.K., R.K. Murray, and M.I. Kotlikoff. 1994. Voltage window for sustained elevation of cytosolic calcium in smooth muscle cells. *Proc. Natl. Acad. Sci. USA.* 91:11914–11918. http://dx.doi.org/10.1073/pnas.91.25.11914

Geary, G.G., D.N. Krause, and S.P. Duckles. 2000a. Estrogen reduces mouse cerebral artery tone through endothelial NOS- and cyclooxygenase-dependent mechanisms. *Am. J. Physiol. Heart Circ. Physiol.* 279:H511–H519.

Geary, G.G., D.N. Krause, and S.P. Duckles. 2000b. Gonadal hormones affect diameter of male rat cerebral arteries through endothelium-dependent mechanisms. *Am. J. Physiol. Heart Circ. Physiol.* 279:H610–H618.

Gonzales, A.L., Y. Yang, M.N. Sullivan, L. Sanders, F. Dabertrand, D.C. Hill-Eubanks, M.T. Nelson, and S. Earley. 2014. A PLCγ1-dependent, force-sensitive signaling network in the myogenic constriction of cerebral arteries. *Sci. Signal.* 7:ra49. http://dx.doi.org/10.1126/scisignal.2004732

Harder, D.R., R. Gilbert, and J.H. Lombard. 1987. Vascular muscle cell depolarization and activation in renal arteries on elevation of transmural pressure. *Am. J. Physiol.* 253:F778–F781.

Hoshi, N., L.K. Langeberg, C.M. Gould, A.C. Newton, and J.D. Scott. 2010. Interaction with AKAP79 modifies the cellular pharmacology of PKC. *Mol. Cell.* 37:541–550. http://dx.doi.org/10.1016/j.molcel.2010.01.014

Ishizaka, N., R.W. Alexander, J.B. Laursen, H. Kai, T. Fukui, M. Oppermann, R.J. Lefkowitz, P.R. Lyons, and K.K. Griendling. 1997. G protein-coupled receptor kinase 5 in cultured vascular smooth muscle cells and rat aorta. Regulation by angiotensin II and hypertension. *J. Biol. Chem.* 272:32482–32488. http://dx.doi.org/10.1074/jbc.272.51.32482

Jaggar, J.H., G.C. Wellman, T.J. Heppner, V.A. Porter, G.J. Perez, M. Gollasch, T. Kleppisch, M. Rubart, A.S. Stevenson, W.J. Lederer, et al. 1998. Ca^{2+} channels, ryanodine receptors and Ca^{2+}-activated K^+ channels: a functional unit for regulating arterial tone. *Acta Physiol. Scand.* 164:577–587. http://dx.doi.org/10.1046/j.1365-201X.1998.00462.x

Jones, T.R., I.H. Kang, D.B. Wheeler, R.A. Lindquist, A. Papallo, D.M. Sabatini, P. Golland, and A.E. Carpenter. 2008. CellProfiler Analyst: data exploration and analysis software for complex image-based screens. *BMC Bioinformatics.* 9:482. http://dx.doi.org/10.1186/1471-2105-9-482

Kanashiro, C.A., and R.A. Khalil. 2001. Gender-related distinctions in protein kinase C activity in rat vascular smooth muscle. *Am. J. Physiol. Cell Physiol.* 280:C34–C45.

Knot, H.J., and M.T. Nelson. 1998. Regulation of arterial diameter and wall [Ca^{2+}] in cerebral arteries of rat by membrane potential and intravascular pressure. *J. Physiol.* 508:199–209. http://dx.doi.org/10.1111/j.1469-7793.1998.199br.x

Lamping, K.G., and F.M. Faraci. 2001. Role of sex differences and effects of endothelial NO synthase deficiency in responses of carotid arteries to serotonin. *Arterioscler. Thromb. Vasc. Biol.* 21:523–528. http://dx.doi.org/10.1161/01.ATV.21.4.523

Li, Y., R.L. Baylie, M.J. Tavares, and J.E. Brayden. 2014. TRPM4 channels couple purinergic receptor mechanoactivation and myogenic tone development in cerebral parenchymal arterioles. *J. Cereb. Blood Flow Metab.* 34:1706–1714. http://dx.doi.org/10.1038/jcbfm.2014.139

Liedtke, W., Y. Choe, M.A. Martí-Renom, A.M. Bell, C.S. Denis, A. Sali, A.J. Hudspeth, J.M. Friedman, and S. Heller. 2000. Vanilloid receptor-related osmotically activated channel (VR-OAC), a candidate vertebrate osmoreceptor. *Cell.* 103:525–535. http://dx.doi.org/10.1016/S0092-8674(00)00143-4

Maddali, K, K., D Korzick D, D Tharp L, and D Bowles K. 2005. PKCδ mediates testosterone-induced increases in coronary smooth muscle $Ca_V1.2$. *Journal of Biological Chemistry.* 280:43024–9.

Mercado, J., R. Baylie, M.F. Navedo, C. Yuan, J.D. Scott, M.T. Nelson, J.E. Brayden, and L.F. Santana. 2014. Local control of TRPV4 channels by AKAP150-targeted PKC in arterial smooth muscle. *J. Gen. Physiol.* 143:559–575. http://dx.doi.org/10.1085/jgp.201311050

Narayanan, D., S. Bulley, M.D. Leo, S.K. Burris, K.S. Gabrick, F.A. Boop, and J.H. Jaggar. 2013. Smooth muscle cell transient receptor potential polycystin-2 (TRPP2) channels contribute to the myogenic response in cerebral arteries. *J. Physiol.* 591:5031–5046. http://dx.doi.org/10.1113/jphysiol.2013.258319

Navedo, M.F., G.C. Amberg, V.S. Votaw, and L.F. Santana. 2005. Constitutively active L-type Ca^{2+} channels. *Proc. Natl. Acad. Sci. USA.* 102:11112–11117. http://dx.doi.org/10.1073/pnas.0500360102

Navedo, M.F., G.C. Amberg, M. Nieves, J.D. Molkentin, and L.F. Santana. 2006. Mechanisms underlying heterogeneous Ca^{2+} sparklet activity in arterial smooth muscle. *J. Gen. Physiol.* 127:611–622. http://dx.doi.org/10.1085/jgp.200609519

Navedo, M.F., G.C. Amberg, R.E. Westenbroek, M.J. Sinnegger-Brauns, W.A. Catterall, J. Striessnig, and L.F. Santana. 2007. $Ca_v1.3$ channels produce persistent calcium sparklets, but $Ca_v1.2$ channels are responsible for sparklets in mouse arterial smooth muscle. *Am. J. Physiol. Heart Circ. Physiol.* 293:H1359–H1370. http://dx.doi.org/10.1152/ajpheart.00450.2007

Navedo, M.F., M. Nieves-Cintrón, G.C. Amberg, C. Yuan, V.S. Votaw, W.J. Lederer, G.S. McKnight, and L.F. Santana. 2008. AKAP150 is required for stuttering persistent Ca^{2+} sparklets and angiotensin II-induced hypertension. *Circ. Res.* 102:e1–e11. http://dx.doi.org/10.1161/CIRCRESAHA.107.167809

Navedo, M.F., E.P. Cheng, C. Yuan, S. Votaw, J.D. Molkentin, J.D. Scott, and L.F. Santana. 2010. Increased coupled gating of L-type Ca^{2+} channels during hypertension and Timothy syndrome. *Circ. Res.* 106:748–756. http://dx.doi.org/10.1161/CIRCRESAHA.109.213363

Nelson, M.T., H. Cheng, M. Rubart, L.F. Santana, A.D. Bonev, H.J. Knot, and W.J. Lederer. 1995. Relaxation of arterial smooth muscle by calcium sparks. *Science.* 270:633–637. http://dx.doi.org/10.1126/science.270.5236.633

Nieves-Cintrón, M., G.C. Amberg, C.B. Nichols, J.D. Molkentin, and L.F. Santana. 2007. Activation of NFATc3 down-regulates the β1 subunit of large conductance, calcium-activated K^+ channels in arterial smooth muscle and contributes to hypertension. *J. Biol. Chem.* 282:3231–3240. http://dx.doi.org/10.1074/jbc.M608822200

Nieves-Cintrón, M., G.C. Amberg, M.F. Navedo, J.D. Molkentin, and L.F. Santana. 2008. The control of Ca^{2+} influx and NFATc3 signaling in arterial smooth muscle during hypertension. *Proc. Natl. Acad. Sci. USA.* 105:15623–15628. http://dx.doi.org/10.1073/pnas.0808759105

Nystoriak, M.A., M. Nieves-Cintrón, and M.F. Navedo. 2013. Capturing single L-type Ca^{2+} channel function with optics. *Biochim. Biophys. Acta.* 1833:1657–1664. http://dx.doi.org/10.1016/j.bbamcr.2012.10.027

Nystoriak, M.A., M. Nieves-Cintrón, P.J. Nygren, S.A. Hinke, C.B. Nichols, C.Y. Chen, J.L. Puglisi, L.T. Izu, D.M. Bers, M.L. Dell'acqua, et al. 2014. AKAP150 contributes to enhanced vascular tone by facilitating large-conductance Ca^{2+}-activated K^+ channel remodeling in hyperglycemia and diabetes mellitus. *Circ.*

Res. 114:607–615. http://dx.doi.org/10.1161/CIRCRESAHA.114.302168

Oppermann, M., N.J. Freedman, R.W. Alexander, and R.J. Lefkowitz. 1996. Phosphorylation of the type 1A angiotensin II receptor by G protein-coupled receptor kinases and protein kinase C. *J. Biol. Chem.* 271:13266–13272. http://dx.doi.org/10.1074/jbc.271.22.13266

Rubart, M., J.B. Patlak, and M.T. Nelson. 1996. Ca^{2+} currents in cerebral artery smooth muscle cells of rat at physiological Ca^{2+} concentrations. *J. Gen. Physiol.* 107:459–472. http://dx.doi.org/10.1085/jgp.107.4.459

Sader, M.A., and D.S. Celermajer. 2002. Endothelial function, vascular reactivity and gender differences in the cardiovascular system. *Cardiovasc. Res.* 53:597–604. http://dx.doi.org/10.1016/S0008-6363(01)00473-4

Sasamura, H., V.J. Dzau, and R.E. Pratt. 1994. Desensitization of angiotensin receptor function. *Kidney Int.* 46:1499–1501. http://dx.doi.org/10.1038/ki.1994.429

Schmied, J.J., M. Raab, C. Forthmann, E. Pibiri, B. Wünsch, T. Dammeyer, and P. Tinnefeld. 2014. DNA origami-based standards for quantitative fluorescence microscopy. *Nat. Protoc.* 9:1367–1391. http://dx.doi.org/10.1038/nprot.2014.079

Sonkusare, S.K., A.D. Bonev, J. Ledoux, W. Liedtke, M.I. Kotlikoff, T.J. Heppner, D.C. Hill-Eubanks, and M.T. Nelson. 2012. Elementary Ca^{2+} signals through endothelial TRPV4 channels regulate vascular function. *Science.* 336:597–601. http://dx.doi.org/10.1126/science.1216283

Sonkusare, S.K., T. Dalsgaard, A.D. Bonev, D.C. Hill-Eubanks, M.I. Kotlikoff, J.D. Scott, L.F. Santana, and M.T. Nelson. 2014. AKAP150-dependent cooperative TRPV4 channel gating is central to endothelium-dependent vasodilation and is disrupted in hypertension. *Sci. Signal.* 7:ra66. http://dx.doi.org/10.1126/scisignal.2005052

Spassova, M.A., T. Hewavitharana, W. Xu, J. Soboloff, and D.L. Gill. 2006. A common mechanism underlies stretch activation and receptor activation of TRPC6 channels. *Proc. Natl. Acad. Sci. USA.* 103:16586–16591. http://dx.doi.org/10.1073/pnas.0606894103

Strotmann, R., C. Harteneck, K. Nunnenmacher, G. Schultz, and T.D. Plant. 2000. OTRPC4, a nonselective cation channel that confers sensitivity to extracellular osmolarity. *Nat. Cell Biol.* 2:695–702. http://dx.doi.org/10.1038/35036318

Tajada, S., P. Cidad, O. Colinas, L.F. Santana, J.R. López-López, and M.T. Pérez-García. 2013. Down-regulation of $Ca_V1.2$ channels during hypertension: how fewer $Ca_V1.2$ channels allow more Ca^{2+} into hypertensive arterial smooth muscle. *J. Physiol.* 591:6175–6191. http://dx.doi.org/10.1113/jphysiol.2013.265751

Teruel, M.N., and T. Meyer. 2000. Translocation and reversible localization of signaling proteins: a dynamic future for signal transduction. *Cell.* 103:181–184. http://dx.doi.org/10.1016/S0092-8674(00)00109-4

Villar, I.C., A.J. Hobbs, and A. Ahluwalia. 2008. Sex differences in vascular function: implication of endothelium-derived hyperpolarizing factor. *J. Endocrinol.* 197:447–462. http://dx.doi.org/10.1677/JOE-08-0070

Wählby, C., I.M. Sintorn, F. Erlandsson, G. Borgefors, and E. Bengtsson. 2004. Combining intensity, edge and shape information for 2D and 3D segmentation of cell nuclei in tissue sections. *J. Microsc.* 215:67–76. http://dx.doi.org/10.1111/j.0022-2720.2004.01338.x

Wellman, G.C., A.D. Bonev, M.T. Nelson, and J.E. Brayden. 1996. Gender differences in coronary artery diameter involve estrogen, nitric oxide, and Ca^{2+}-dependent K^+ channels. *Circ. Res.* 79:1024–1030. http://dx.doi.org/10.1161/01.RES.79.5.1024

Welsh, D.G., A.D. Morielli, M.T. Nelson, and J.E. Brayden. 2002. Transient receptor potential channels regulate myogenic tone of resistance arteries. *Circ. Res.* 90:248–250. http://dx.doi.org/10.1161/hh0302.105662

Zhao, L., M.N. Sullivan, M. Chase, A.L. Gonzales, and S. Earley. 2014. Calcineurin/nuclear factor of activated T cells-coupled vanilliod transient receptor potential channel 4 Ca^{2+} sparklets stimulate airway smooth muscle cell proliferation. *Am. J. Respir. Cell Mol. Biol.* 50:1064–1075. http://dx.doi.org/10.1165/rcmb.2013-0416OC